Bioorganic Chemistry 108 (2021) 104615

Contents lists available at ScienceDirect

Bioorganic Chemistry

journal homepage: www.elsevier.com/locate/bioorg

Eco-friendly sequential one-pot synthesis, molecular docking, and anticancer evaluation of arylidene-hydrazinyl-thiazole derivatives as CDK2 inhibitors

Abeer M. El-Naggar [a,*], Maher A. El-Hashash [a], Eslam B. Elkaeed [b,c,*]

[a] Department of Chemistry, Faculty of Science, Ain Shams University, Abbassiya 11566, Cairo, Egypt
[b] Department of Pharmaceutical Sciences, College of Pharmacy, AlMaarefa University, Ad Diriyah 13713, Riyadh, Saudi Arabia
[c] Department of Pharmaceutical Organic Chemistry, Faculty of Pharmacy (Boys), Al-Azhar University, Nasr City 11884, Cairo, Egypt

ARTICLE INFO

Keywords:
Arylidene-hydrazinyl-thiazole
Cyclin-dependent kinases (CDK)
Roscovitine
CDK2 inhibitor
Anti-proliferative
Cell cycle
Apoptosis
Docking

ABSTRACT

One current approach in the treatment of cancer is the inhibition of cyclin dependent kinase (CDK) enzymes with small molecules. CDK are a class of enzymes, which catalyze the transfer of the terminal phosphate of a molecule of ATP to a protein that acts as a substrate. Among CDK enzymes, CDK2 has been implicated in a variety of cancers, supporting its potential as a novel target for cancer therapy across many tumor types. Here the discovery and development of arylidene-hydrazinyl-thiazole as a potentially CDK2 inhibitors is described, including details of the design and successful synthesis of the series analogs (**27a-r**) using one-pot approach under eco-friendly ultrasound and microwave conditions. Most of the newly synthesized compounds showed good growth inhibition when assayed for their *in-vitro* anti-proliferative activity against three cancer cell lines (HepG2, MCF-7 and HCT-116) compared to the reference drug roscovitine, with little toxicity on the normal fibroblast cell lines (WI-38). Furthermore, the compounds exhibiting the highest anti-proliferative activities were tested against a panel of kinase enzymes. These derivatives displayed an outstanding CDK2 inhibitory potential with varying degree of inhibition in the range of IC_{50} 0.35–1.49 μM when compared with the standard inhibitor roscovitine having an IC_{50} value 0.71 μM. The most promising CDK2 inhibitor (**27f**) was selected for further studies to determine its effect on the cell cycle progression and apoptosis in HepG2 cell line. The results indicated that this compound implied inhibition in the G2/M phase of the cell cycle, and it is a good apoptotic agent. Finally, Molecular docking study was performed to identify the structural elements which involved in the inhibitory activity with the prospective target, CDK2, and to rationalize the structure-activity relationship (SAR).

1. Introduction

Cancer is increasingly a global health issue and affects millions of people of all ages around the world. In 2018, nearly 18.1 million people were diagnosed with cancer, of which 9.6 million people died [1]. The national cancer institute projects that by the year 2030, 23.6 million people may get affected with cancer of which 14 million people may die. Cancer is a genetic disease; it arises due to genetic alterations/mutations in protooncogenes and/or tumor suppressor genes [2]. Proto-oncogenes are genes that help to regulate cell growth and differentiation, when they are mutated, they can become oncogenes leading to their unregulated expression in a normal cell transforming them into a cancerous cell [3].

A greater understanding of cancer biology will open the door to the development of new therapeutic options to combat cancer. Increasingly it has become recognized that aberration of cell cycle checkpoints constitutes a hallmark of cancer [4]. Progression through the various phases of the eukaryotic cell cycle relies upon the sequential activation and inactivation of a number of important enzymes called cyclin-dependent kinases (CDKs). CDKs are a small subgroup of a larger family of enzymes, called protein kinases, which catalyze the transfer of a phosphate group from adenosine triphosphate to specific serine (Ser) and threonine (Thr) residues on proteins involved in cell proliferation. CDKs are not active by themselves and must be bound with a second type of protein, cyclin, in addition to being phosphorylated in order to achieve full enzymatic activity [5,6]. Tumor development is closely associated with genetic

* Corresponding authors.
E-mail addresses: elsayedam@sci.asu.edu.eg (A.M. El-Naggar), eslamkaeed@azhar.edu.eg (E.B. Elkaeed).

https://doi.org/10.1016/j.bioorg.2020.104615
Received 20 September 2020; Received in revised form 19 November 2020; Accepted 28 December 2020
Available online 5 January 2021

alterations and deregulation of CDKs and their regulators, the cyclins.

To date, twenty CDKs and at least 29 cyclin proteins have been identified in humans and only a certain subset of CDK-cyclin complexes is directly involved in driving the cell cycle [7]. CDK2/Cyclin A complex is often used as prototypes for the major classes of regulatory pathways that control CDK activity [8]. CDK2 has been shown overexpressed in several tumors, such as hepatocellular carcinoma, lung carcinoma, melanoma, osteosarcoma, ovarian carcinoma, breast cancer and pancreatic cancer [9,10]. The expression of active CDK2/Cyclin A complex by injection led to the effective ablation of G2 phase and caused cells to display mitotic abnormalities [11]. Hence, CDK2 is considered a good candidate target for novel valid therapeutic approaches against different types of cancer [12].

Several CDK inhibitors have been developed as potential anticancer agents. First-generation compounds, which include pan-CDK inhibitors such as UCN-01 (**1**), flavopiridol (**2**), olomoucine (**3**) and (R)-roscovitine (**4**) (Fig. 1), generally showed low activity and/or high toxicity in the clinical trials [13–15].

Second-generation CDK inhibitors can be grouped into three different classes: I) Compounds with a broad CDK activity spectrum, such as SNS-032 (**5**) and R547 (**6**) [16–18]. II) Compounds with preferential CDK4/CDK6- or CDK2-inhibitory activity, such as AT-7519 (**7**, CDK2) and P276-00 (**8**, CDK4/CDK6) [13,19–21]. III) Compounds with CDK-inhibitory activity and off-kinase targets, which can be exploited to enhance their anticancer activity. This class includes ZK-304709 (**9**, CDK/VEGFR activity) and JNJ-7706621 (**10**, CDK/Aurora A and B activity) (Fig. 2) [22–24]. Compound 7 is FDA approved in 2015 for treatment of breast cancer.

There are many studies supporting the idea of targeting CDK2 to control cancer progression [25].

In this paper, we describe the synthesis and evaluation of arylidene-hydrazinyl-thiazole derivatives as a potential CDK2 inhibitors. The target compounds were synthesized based on sequential one-pot reactions that exhibit several advantages, including avoid the isolation of intermediates, prevention of time-consuming multi-steps purification, and the overall yields of such processes are found to be higher [26,27].

1.1. Rational drug design

The interactions of the ATP-competitive CDK2 inhibitors are reported for several compounds. For example, NU2058 (**11**) was shown to bind the CDK2/Cyclin A complex via a triplet of hydrogen bonds between the purine base and the CDK2 hinge region. The cyclohexylmethoxy moiety was shown to interact with the ribose-binding pocket, whilst the imidazole ring of the purine makes a π-π interaction with the Phe80 residue (Fig. 3) [28].

Structure-activity relationship (SAR) studies revealed that the purine pharmacophore was not a prerequisite for CDK2-inhibitory activity [29]. In an attempt to maintain the H-bond interactions observed for NU2058 (**11**), the pyrimidine NU6027 (**12**) was first identified. The established SAR for this chemotype can be represented as in Fig. 4. As for NU2058 (**11**), the pyrimidine NU6027 (**12**) displayed a competitive behavior on CDK2 with respect to ATP [29].

Our lead compound was the commercially available CDK2 inhibitor, roscovitine (**4**), also known as seliciclib. Docking studies revealed that roscovitine indeed occupied the ATP binding site of CDK2 and the 2 nitrogen atoms of the donor-acceptor motif generates two hydrogen bonds with Leu83 of the hinge region. The isopropyl moiety occupied a narrow hydrophobic pocket formed by hydrophobic residue, and the benzyl ring of roscovitine is directed towards the solvent-accessible region of the kinase, facing the outside of the ATP-binding pocket and forming 20 van der Waal's contacts with mainly Ile10, Phe82 and His84. (Fig. 5) [30].

Based on the studies on roscovitine, new investigation focused on developing more selective CDK inhibitors with increased selectivity towards CDK2 (compounds **13**–**22**, Fig. 6) [31–38]. These inhibitors are developed based on two major approaches [39]: I) changing the purine base into other bioisosteres motifs, such as guanine, pyrimidine, imidazole, pyrazole, and thiazole derivatives, II) changing the ratios and positions of carbon and nitrogen atoms attached to the heterocyclic core, III) using combinations of the two approaches.

Although many CDK2 inhibitors appeared to be promising in preclinical studies, only few progressed past Phase I clinical trials, for example, dinaciclib was the most extensively studied. It is a potent inhibitor of CDK2 (1–4 nM) which inhibited cell cycle on a number of different cancer cell lines [40]. It also caused regression of tumors in mouse models. Following this, phase I studies provided encouraging results; however, phase II studies failed to support its use in clinic. Other CDK2 inhibitors that were developed and tested such as AT7519, a pyrazole 3-carboxyamide compound, and AZD5438, failed to achieve the desired clinical outcome [13,41].

Among several classes of potential CDK2 inhibitors, we focused our attention on arylidene hydrazinyl-thiazole derivatives because of the low molecular weight of the scaffold and amenability for rapid class expansion, in addition to the presence of the essential pharmacophoric features required for binding with CDK2 as shown in Fig. 7. The substituents flanking the thiazole core occupy the shallow hydrophobic pocket on one end and the aromatic moiety are pointed out towards the solvent exposed area on the other end. The hydrazinyl-thiazole moiety contains three heteroatoms that are capable of forming a network of hydrogen bonds with the hinge region of the kinase backbone.

Depending on the previous discussion and our work to develop kinase inhibitors as an anticancer agents [42,43], and in addition to our efforts in syntheses of heterocyclic compounds, anticipated biological activity, under green chemistry [44–46], a series of arylidene-hydrazinyl-thiazole derivatives were designed, synthesized under green conditions, and evaluated for their cytotoxicity against HepG2, MCF-7, HCT-116, and Wi-38 cancer cell lines. The possible mechanisms of cytotoxicity action of the most active compounds were further studied through *in vitro* Kinase enzymatic assay. The cell phase which may be

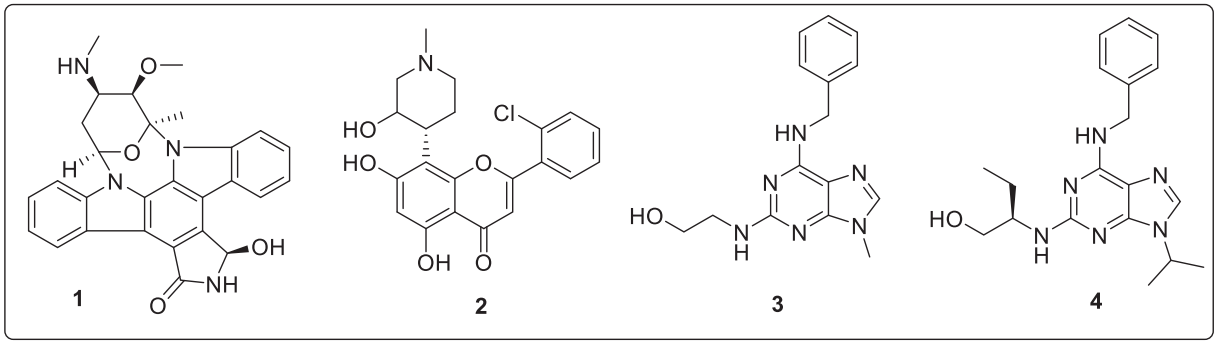

Fig. 1. UCN-01 (**1**), Flavopiridol (**2**), olomoucine (**3**) and (R)-roscovitine (**4**).

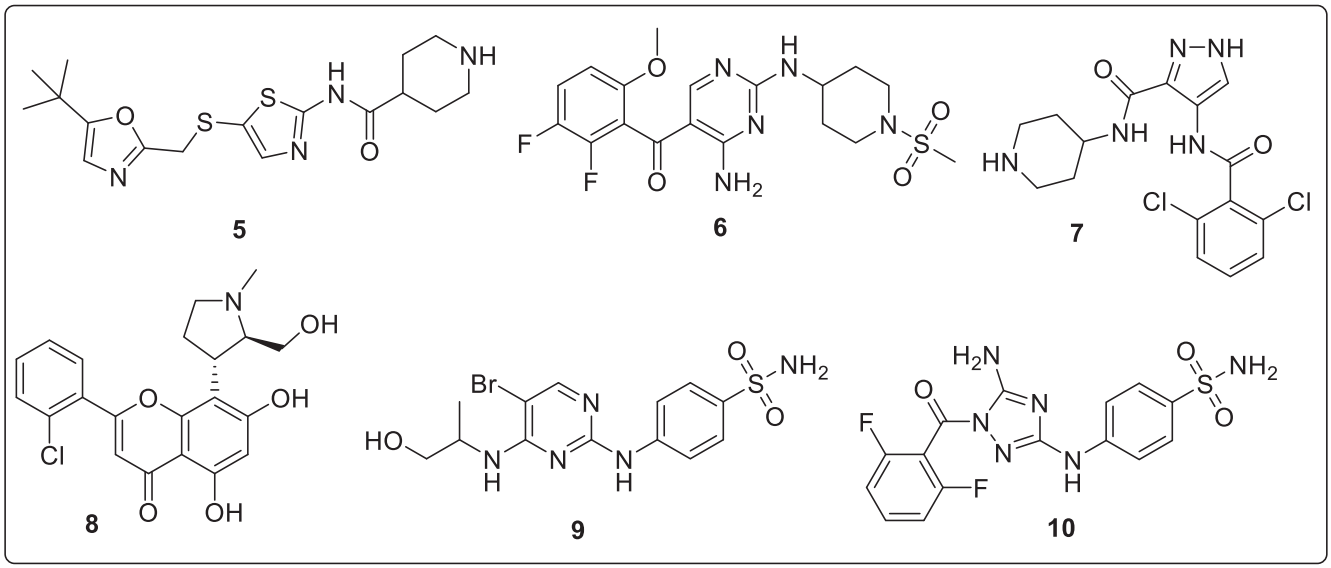

Fig. 2. SNS-032 (**5**), R547 (**6**), AT-7519 (**7**), P276-00 (**8**), ZK-304709 (**9**) and JNJ-7706621 (**10**).

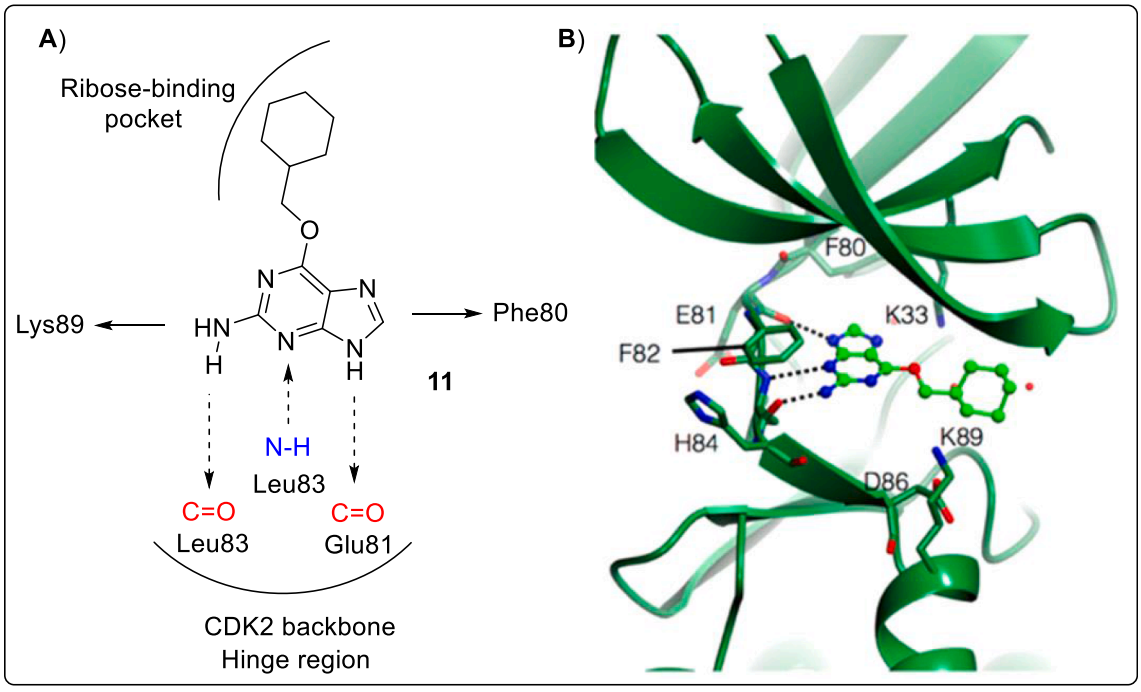

Fig. 3. ***(A)*** *CDK2-NU2058* ***(11)*** *interactions.* ***(B)*** *CDK2-NU2058* ***(11)*** *complex* [28]

arrested by the most active compound was determined by cell cycle assay. Finally, inhibitor molecular docking study, utilizing the crystal structure of CDK2 kinase domain, of the active compounds was performed to investigate their binding patterns with the potential CDK2 target.

2. Results and discussion

2.1. Chemistry

A new series of arylidene-hydrazinyl-thiazole derivatives (**27a–r)** was prepared in two consequence steps as shown in Scheme 1. Firstly, by condensation of aryl ketones **23a-f** with thiosemicarbazide (**24**) to afford arylidene-thiosemicarbazones (schiff's base **25a-f).** The second step of this synthetic route involved the cyclization of schiff's base **25a-f** in the same vessel with α-halocarbonyl derivatives **26a–d**. From the first step it was also possible to isolate the reaction intermediate **25a**. Both the condensation and cyclization reactions were performed by the Hantzsch protocol, under two, ultrasonic and microwave, green conditions.

A possible mechanism for the preparation of the target compounds **27a-r** is speculated and described in Scheme 2. The first step is the activation of aryl ketones **23a-f** for nucleophilic attack by thiosemicarbazide **24** with drops of glacial acetic acid under both ultrasonic condition and microwave irradiation. The formed key intermediate, thiosemicarbazones **25a-f,** is treated with α-halocarbonyl derivatives where the nucleophilic sulfur displaced the chloride atom. The formed intermediate product is then cyclized with the elimination of water

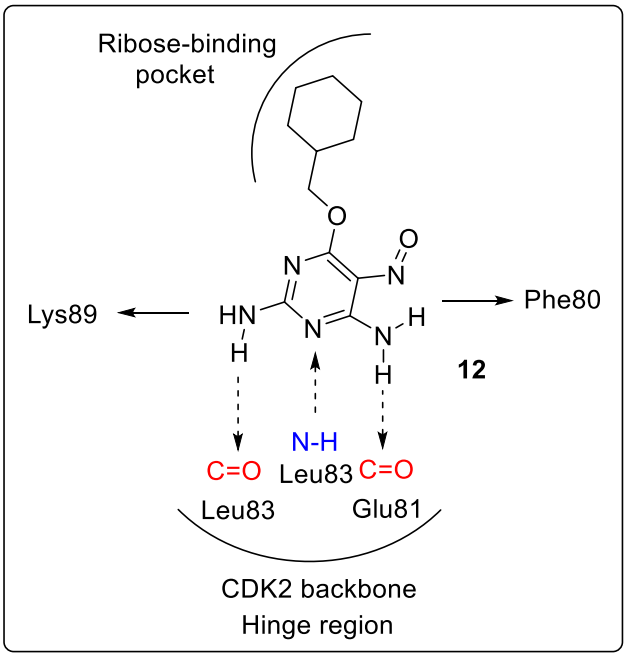

Fig. 4. CDK2-NU6027 (**12**) interactions.

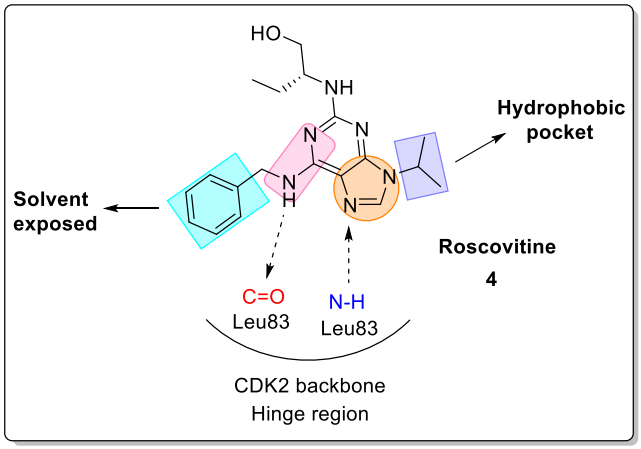

Fig. 5. Schematic drawing of cdk2 interactions with roscovitine (**4**).

molecule and rearranged to generate the aromaticity and allows the formation of the desired compounds, arylidene-hydrazinyl-thiazole (**27a-r**).

To our delight, this successive method was appeared to be clean and formed the desired product **27a-r** in high yield. In comparison between the two techniques, it was observed that the reaction yield and time under microwave irradiation are better than under ultrasonic. In MW irradiation, the reaction yield increased from (55–79%) to (88–95%), also the time of the reaction decreased from 20 min to 4 min (Table 1).

Structures **27a-r** were established based on spectral data. IR spectra revealed absorption bands at the ranges 3215–3426, 1649–1684 and 1611–1628 cm^{-1} for (NH) and (C═$O_{(acetyl)}$) and C═N groups, respectively. The ^{1}H NMR spectrum of **27a-r** show the characteristic peak due to imine methyl protons between 2.22 ppm and 3.45 ppm and the aromatic phenyl ring protons resonate between 6.55 ppm and 8.25 ppm. The ^{13}C NMR and Mass spectra of compounds provided additional evidence in support of the proposed structures.

2.2. Biological evaluation

2.2.1. In vitro anti-proliferative activities

The anti-proliferative activities of the synthesized compounds were confirmed conducting studies on hepatocellular carcinoma (HepG2), human breast adenocarcinoma (MCF-7) and colon carcinoma (HCT-116) in addition to normal fibroblasts (WI-38) cell lines, with roscovitine serving as control compound. Results showed that all the synthesized analogs exhibited weak to excellent activities as shown in Table 2. Among the three cell lines, HepG2 cells were the most sensitive to compounds **27a**, **27c**, **27f**, **27j**, **27n**, and **27q**, whereas MCF-7 and HCT-116 cells were more responsive to compounds **27g** and **27n** treatment as evident by lower IC_{50} values. All the most active compounds showed a little toxicity on the non-cancerous cells (WI-38).

2.2.2. Kinase inhibitory assay

Selected compounds (**27a**, **27c**, **27f**, **27g**, **27j**, **27k**, **27n** and **27q**) exhibiting the highest anti-proliferative activities were further tested for their kinase inhibitory potential against CDK1, CDK2 and EGFR enzymes. All analogs showed a varied degree of CDK2 inhibitory potential with IC_{50} values ranging between 0.35 and 1.49 μM when compared with roscovitine as standard drug (IC_{50} = 0.71 μM) (Table 3). Compound **27f**, containing furan ring in the hydrophobic tail, demonstrated the highest activity and was two folds more potent (0.35 μM vs 0.71 μM) than the standard competitive inhibitor roscovitine against CDK2. The second most active compound in this series, **27 g** which inhibit CDK2 kinase with IC_{50} of 0.37 μM. This assay proves that our compounds indeed possess the capacity to inhibit the CDK2 kinase at as low as submicromolar concentration in comparable to CDK1 and EGFR kinase enzymes.

2.2.3. In-vitro DNA-flow cytometric (cell cycle) analysis

The CDK family has been extensively studied for its regulation of all phases of the cell cycle. Also, it has been reported that roscovitine is suggested to cause cell cycle arrest in the G1 and G2/M phases [47]. Having shown that **27a-r** effectively targets CDK2 and also decreases cell growth, we sought to understand how it may alter cell cycle progression. The most active CDK2 inhibitor compound was **27f**, and this compound was used for the cell cycle analysis. HepG2 cells were treated with DMSO, roscovitine or **27f** for 48 h at different concentration and then analyzed for DNA content by flow cytometry. The results from this experiment are summarized in Figs. 8 and 9. It was clearly that compound **27f** effectively arrested the HepG2 cells in G2/M phase of the cell cycle which is consistent with the previous findings that CDK2 regulates the G2/M checkpoint [11,48].

2.2.4. Determination and assay of apoptosis using Annexin V-FITC staining.

The mode of cell death induced by compound **27f** was further investigated to determine whether death is due to apoptosis or necrosis. As roscovitine can induce cancer cell apoptosis [49], the apoptotic nature of compound **27f** against HepG2 cells was evaluated via flow cytometry detection using AnnexinV-FITC and PI double staining. The results shown in Fig. 10 revealed that application of compound **27f** on HepG2 cells for 48 h at 1 μM concentration, increases the early apoptosis ratio (lower right quadrant of the cytogram) from 0.41% to 2.82%, and increases the late apoptosis ratio (upper right quadrant of the cytogram) from 0.19% to 10.79%. Moreover, the apoptosis ratio was also investigated at higher concentration (10 μM) for both roscovitine as a reference and **27f** (Fig. 11). All the results indicate that compound **27f** could induce apoptosis in cancer cells.

The biological results were also supported by docking studies, which are described in the following section.

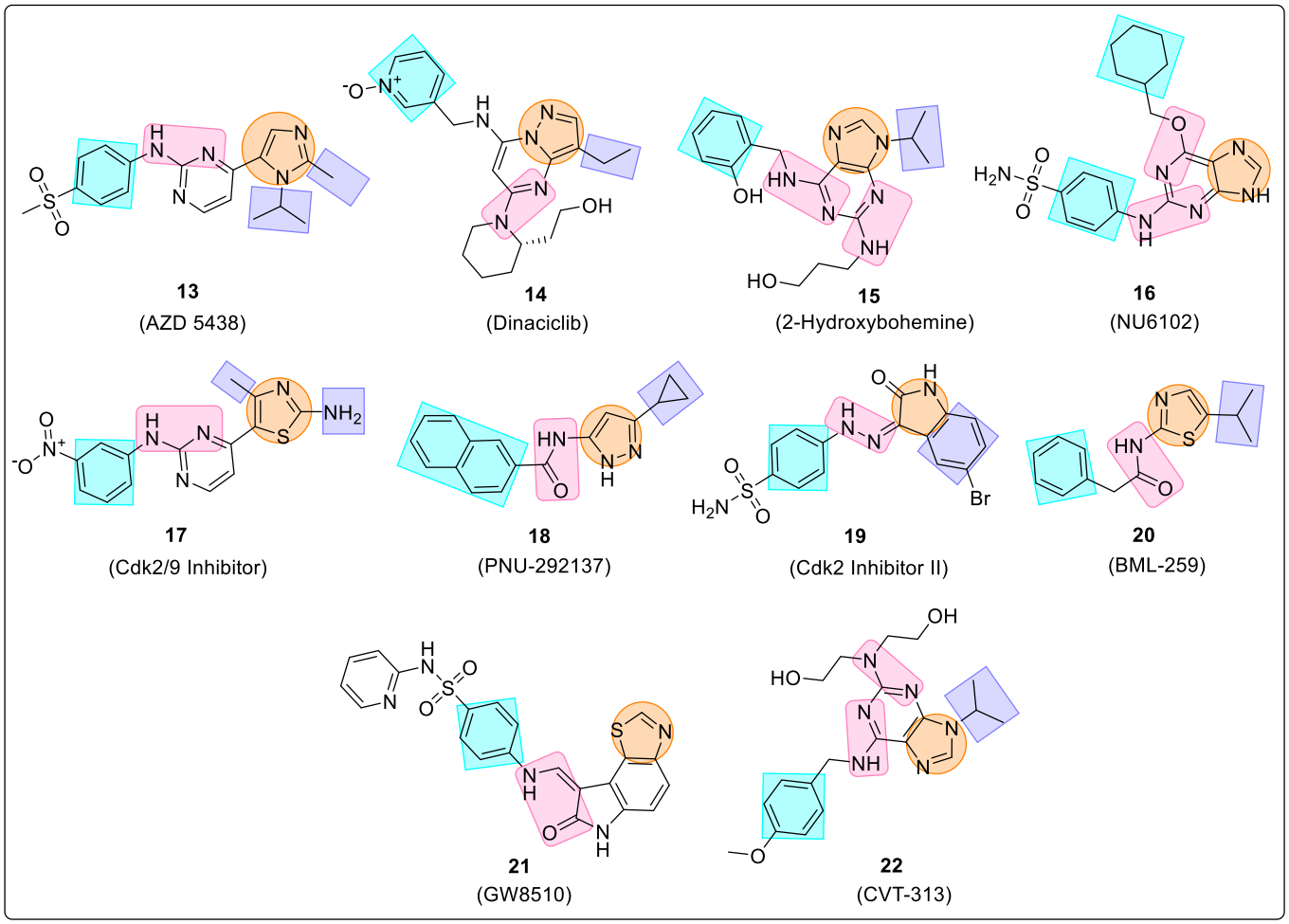

Fig. 6. Examples of structural motifs of known purine and other bioisosteres (**13**–**22**) designed as CDK2 inhibitors.

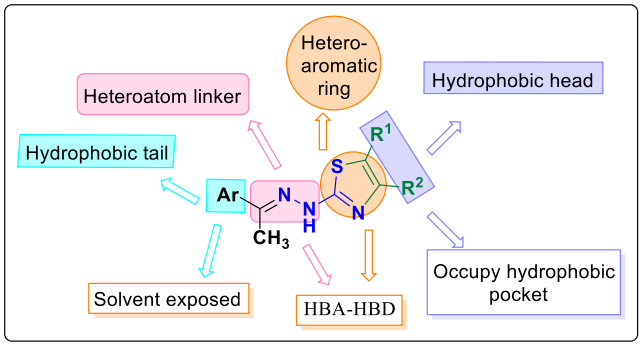

Fig. 7. Rational of molecular design of the new proposed CDK2 inhibitors.

2.3. Docking studies

The docking is a significant tool to explore the interactions between an inhibitor and the target [50]. To find the binding interactions of the synthesized compounds in the active sites of the CDK2 kinase, the MOE-Dock program (www.chemcomp.com) was used to perform molecular docking. The 3D crystal structure of the CDK2 kinase domain complexed with roscovitine was retrieved from the Protein Databank (PDB ID: 2A4L) since it has the highest resolution (2.4 Å) among all the CDK2 crystal structures. The synthesized compounds were docked into the active site of the target enzyme in MOE by the default parameters, and the top ranked conformation based on docking score was selected for further studies in molecular docking.

Docking studies suggested that arylidene-hydrazinyl-thiazole well accommodate inside the active site of CDK2 enzyme and involved different interactions with enzyme Lys89, His 84, Glu8, Ile10, Gln131, Leu134, and Leu83, etc. Docking score and interactions are listed in the Table 4.

Compounds that have interesting biological results, either in the anti-proliferative activities or in the CDK2 inhibitory assay, show very good potential result against CDK2 with regard to roscovitine. Compound **27f** with docking score of −18.63 show very good potential against CDK2 enzyme (Figs. 12 and 13) almost similar to roscovitine score (-17.03). Lys89 amino acid was observed making an electrostatic interaction involving two hydrogen bonds with the thiazole N and hydrazinyl N atoms of **27f**. It is also possible that the methyl group attached to thiazole ring can form favorable interactions in the active site of CDK2, possibly a hydrophobic interaction with His84.

Compound **27 g** showed very good inhibitory effect against CDK2 enzyme (Figs. 14 and 15). This compound has the potential to form two hydrogen bonds in the active site with Lys89 similar to compound **27f**, as well as having an extension with the potential to make very strong hydrophobic interactions with the ATP cleft of the active site between the methyl groups and the Leu134, Ile10 amino acids. Moreover, the furan ring is extended in the pocket to form hydrophobic interaction with the surrounding Glu8 and His84 amino acids.

Compound **27c** showed some interaction with CDK2 enzyme in different pattern (Figs. 16 and 17). The electron cloud system of thiazole ring was able to form arene-cation interaction with Lys89 amino acid residue. Also, the NH of the hydrazinyl moiety can function as hydrogen

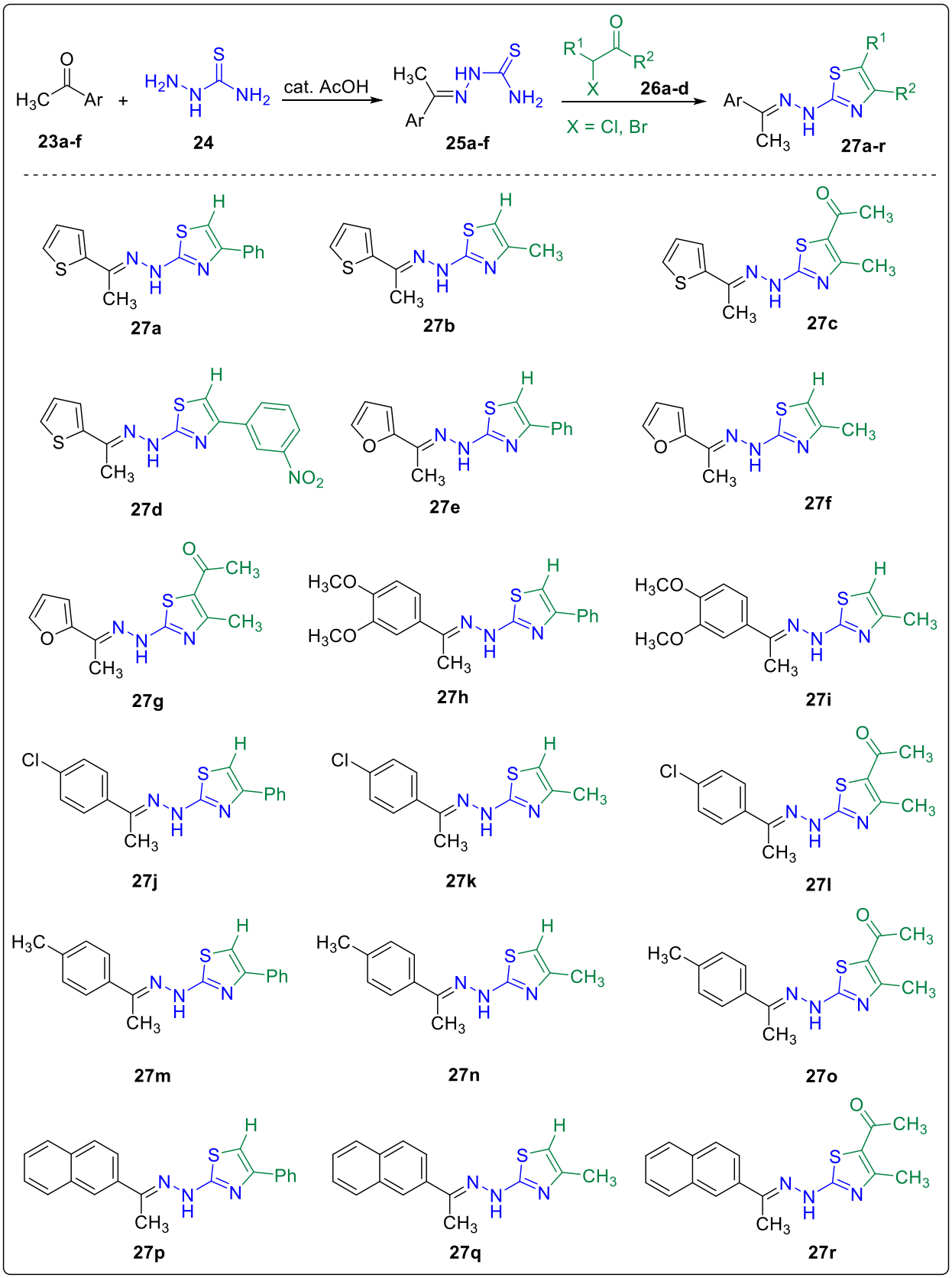

Scheme 1. Synthesis of compound **27a-r.**

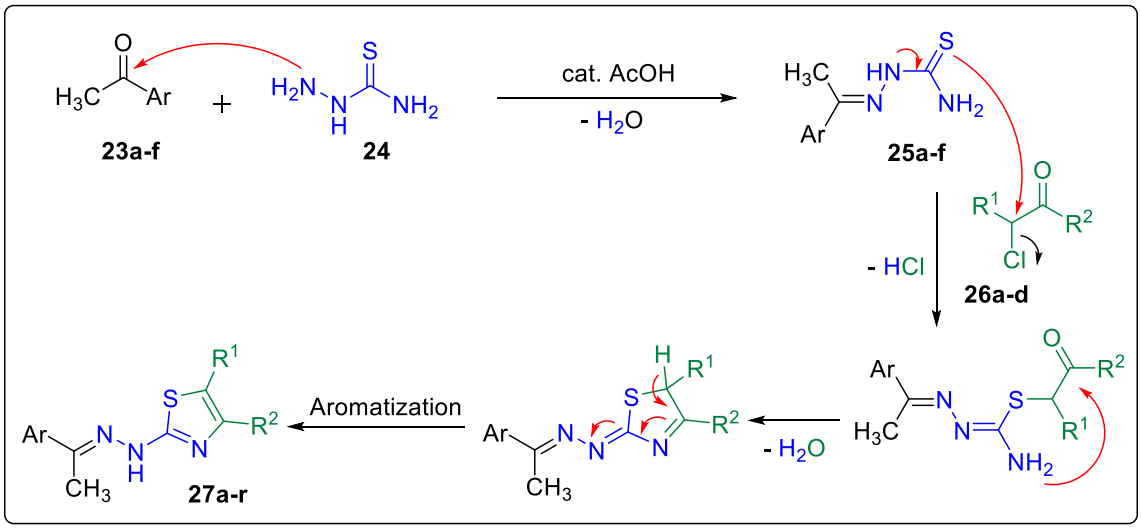

Scheme 2. Proposed reaction mechanism for compounds **27a-r** formation.

Table 1
Comparative yield of ultrasonic (US) and microwave (MW) methods for the synthesis of compounds **27a-r.**

Compound no.	Yield of 2 steps (one-pot reaction)	
	***US (%)Step 1:** 5 mins**Step 2:** 15 mins*	***MW (%)Step 1:** 2 mins**Step 2:** 2 mins*
27a	79	94
27b	55	93
27c	62	95
27d	60	90
27e	78	91
27f	77	88
27g	79	90
27h	79	90
27i	79	90
27j	77	94
27k	55	93
27l	60	90
27m	62	95
27n	78	91
27o	54	92
27p	77	94
27q	55	93
27r	60	90

Table 2
In vitro anti-proliferative activities towards HepG2, MCF-7, HCT-116 and WI-38 cell lines.

Compound	IC_{50} (μM)[a]			
	HepG2	**MCF-7**	**HCT-116**	**WI-38**
27a	9.06 ± 0.9	18.48 ± 1.8	26.07 ± 1.9	42.13 ± 2.9
27b	34.65 ± 2.6	53.76 ± 3.7	63.39 ± 3.8	86.24 ± 4.3
27c	10.35 ± 1.1	19.18 ± 1.8	30.67 ± 2.2	80.13 ± 4.0
27d	48.17 ± 3.4	50.22 ± 3.5	56.52 ± 3.5	38.54 ± 2.6
27e	39.73 ± 2.8	67.37 ± 4.0	77.38 ± 4.3	64.92 ± 3.7
27f	8.49 ± 0.7	17.09 ± 1.5	22.50 ± 1.7	73.45 ± 3.9
27g	43.85 ± 3.1	8.97 ± 0.7	10.89 ± 1.0	37.86 ± 2.7
27h	52.13 ± 3.4	82.32 ± 4.9	93.16 ± 5.2	>100
27i	31.48 ± 2.2	45.66 ± 3.3	49.68 ± 3.2	61.87 ± 3.5
27j	6.48 ± 0.5	16.28 ± 1.4	18.82 ± 1.4	34.17 ± 2.5
27 k	19.59 ± 1.7	37.31 ± 2.9	42.16 ± 2.9	55.63 ± 3.4
27 l	57.61 ± 3.6	41.29 ± 3.2	51.33 ± 3.4	11.39 ± 1.1
27m	69.23 ± 4.0	15.17 ± 1.2	80.23 ± 4.6	35.28 ± 2.3
27n	5.16 ± 0.3	9.23 ± 0.8	13.71 ± 1.1	47.16 ± 3.1
27o	28.20 ± 2.0	32.45 ± 2.6	36.34 ± 2.6	23.02 ± 1.9
27p	58.02 ± 3.8	27.25 ± 2.5	44.24 ± 2.9	29.50 ± 2.2
27q	14.27 ± 1.3	23.94 ± 2.1	32.12 ± 2.5	NT[b]
27r	65.19 ± 3.9	59.81 ± 3.8	71.51 ± 3.9	25.41 ± 2.0
Roscovitine	**13.82 ± 1.15**	**9.32 ± 0.49**	**12.24 ± 1.17**	**17.31 ± 1.05**

[a] IC_{50} values are the mean ± S.D. of three separate experiments; IC_{50} (μM): 1–10 (very strong), 11–20 (strong), 21–50 (moderate), 51–100 (weak), more than 100 (non-cytotoxic).
[b] NT: Compounds not tested for their anti-proliferative activities.

bond acceptor forming a hydrogen bond with Leu83 backbone.

It would appear from these results that the ability to form two hydrogen bonds or one hydrogen bond and arene-cation interaction in the active site considered so crucial in the design of the molecules. Fig. 18 illustrate this crucial requirement for other selected docked CDK2 inhibitors (**27a**, **27j**, **27 m** and **27q**).

3. Structure-activity relationships (SAR)

The structure-activity relationship was mainly based upon by bring about difference of substituent in the hydrophobic head and hydrophobic tail in the synthesized compounds. The incorporation of the bulky lipophilic extension, methyl and phenyl group in the hydrophobic head of compounds **27a**, **27c**, **27f**, **27 g**, **27j**, vastly increased the inhibitory effect of the molecule by binding with the lipophilic pocket in the target binding site.

Also, the structure-activity relationship studies on the arylidene-hydrazinyl-thiazole series revealed that the purine pharmacophore in roscovitine is not a prerequisite for CDK2-inhibitory activity. The nitrogen atoms and their position in the hydrazinyl linker and thiazole ring can do the same role of the purine ring by occupying the hinge region and function as hydrogen bond donor (e.g. **27a**, **27f**, **27 g**, **27 m**, **27q**) or hydrogen bond acceptor (e.g. **27a**, **27c**, **27j)** enabling them to compete with ATP in the hinge region of the kinase backbone.

In addition to the capacity of the hydrazinyl linker to form network of hydrogen bonds, it possibly provide an extra chain length that allows more flexibility to fit into the binding pocket more effectively, so these would be the logical reason for the improvement in activity for the whole arylidene-hydrazinyl-thiazole series.

Lack of the hydrophobic head in the non-cyclized intermediate **25a** , showed decreased binding affinity with CDK2 kinase. Also, the decline in the CDK2 assay inhibitory activity in compound **27d** is probably due to the incorporation of strong nitro electron withdrawing group in the hydrophobic head attached to the thiazole ring. Therefore, the hydrophobic head with high electron system is essential for the activity.

Table 3
In vitro enzymatic inhibitory activities of arylidene-hydrazinyl-thiazoles against CDK2, CDK1 and EGFR.

Compound	**CDK2** (IC_{50}, μM)	CDK1 (IC_{50} ,μM)	EGFR
27a	0.73 ± 0.022	15.99 ± 0.8	23.37 ± 1.20
27b	NT[a]	NT[a]	NT[a]
27c	0.39 ± 0.009	22.08 ± 1.1	62.06 ± 3.14
27d	NT[a]	NT[a]	NT[a]
27e	NT[a]	NT[a]	NT[a]
27f	**0.35** ± 0.008	31.63 ± 1.6	99.82 ± 5.06
27g	0.37 ± 0.008	29.77 ± 1.5	45.11 ± 2.27
27h	NT[a]	NT[a]	NT[a]
27i	NT[a]	NT[a]	NT[a]
27j	**0.56** ± 0.014	36.23 ± 1.8	14.67 ± 0.76
27k	1.27 ± 0.032	90.57 ± 4.6	70.28 ± 3.57
27l	NT[a]	NT[a]	NT[a]
27m	NT[a]	NT[a]	NT[a]
27n	1.49 ± 0.038	70.06 ± 3.5	216.63 ± 11.04
27o	NT[a]	NT[a]	NT[a]
27p	NT[a]	NT[a]	NT[a]
27q	1.43 ± 0.040	29.74 ± 1.5	21.43 ± 1.10
27r	NT[a]	NT[a]	NT[a]
Roscovitine	**0.71** ± 0.004	22.90 ± 1.5	30.40 ± 1.55

[a] NT: Compounds not tested for their kinase inhibitory assay

4. Conclusion

In summary, we have synthesized eighteen arylidene-hydrazinyl-thiazole analogs (**27a-r**) under eco-friendly synthetic conditions. The target compounds were obtained in 4 mins with an excellent yield using microwave irradiation. All the synthesized compounds were found to inhibit the proliferation and induce cytotoxicity toward HepG2, MCF-7 and HCT-116 cell lines, in a varied degree when compared with standard drug, roscovitine. Most of the tested compounds showed significant activity in CDK2 enzymatic assay and were found to be equivalent or even more potent than roscovitine. In particular, compound **27f** demonstrated the highest activity and was twice fold more potent than the parent CDK2 inhibitor, roscovitine. Additionally, compound **27f** was shown to induce cell cycle arrest in the G2/M phase of HepG2 cell lines. **27f** also exhibited apoptotic effects against these cell lines, as shown by the increased number of cells in the early and late stages of apoptosis. Molecular docking studies were carried out in order to rationalize the results. SAR studies demonstrated that the inhibitory activity for this set of compounds is consistent with the presence of the key hydrogen bond interactions made by the heteroatom linker and thiazole ring within the CDK2 hinge region. Also, the hydrophobic interactions between the hydrophobic head, attached to the thiazole ring, and the surrounding amino acids residues was crucial for the activity.

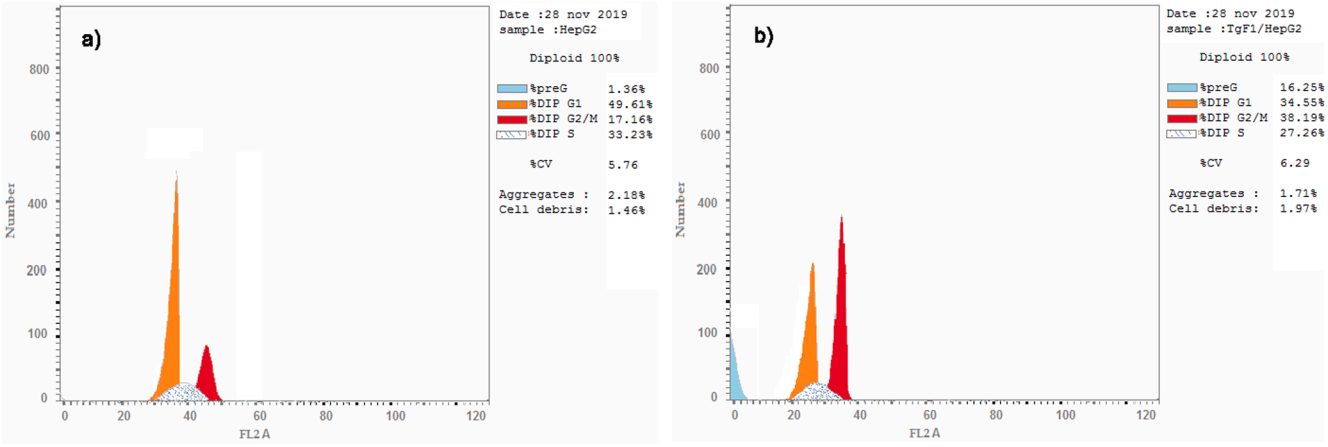

Fig. 8. a) Cell cycle analysis of HepG2 cells treated with DMSO as a control for 48 h; b) Cell cycle analysis of HepG2 cells treated with compound **27f (**1 μg/mL concentration) for 48 h.

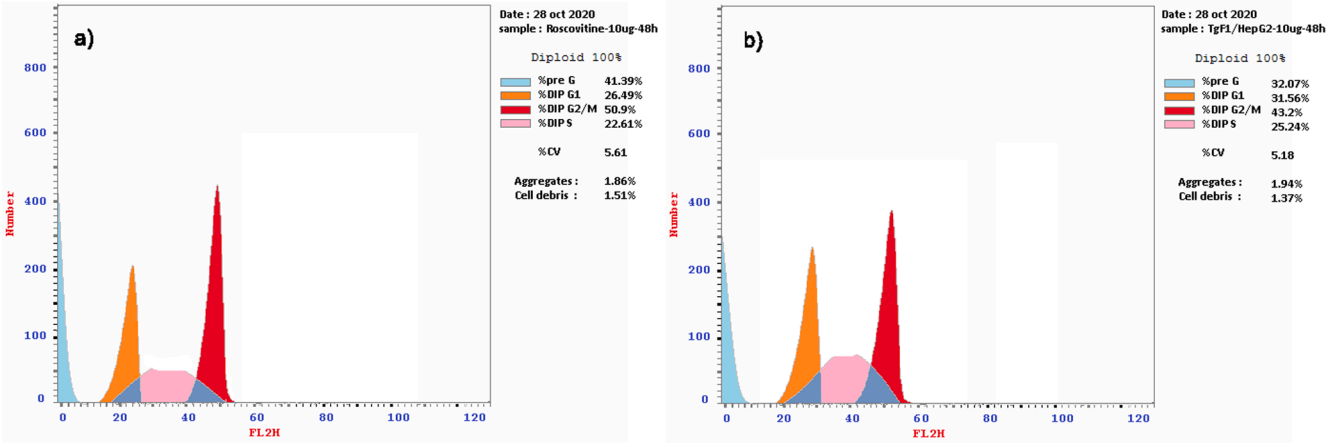

Fig. 9. a) Cell cycle analysis of HepG2 cells treated with **Roscovitine** as a reference (10 μg/mL concentration) for 48 h; b) Cell cycle analysis of HepG2 cells treated with compound **27f** (10 μg/mL concentration) for 48 h.

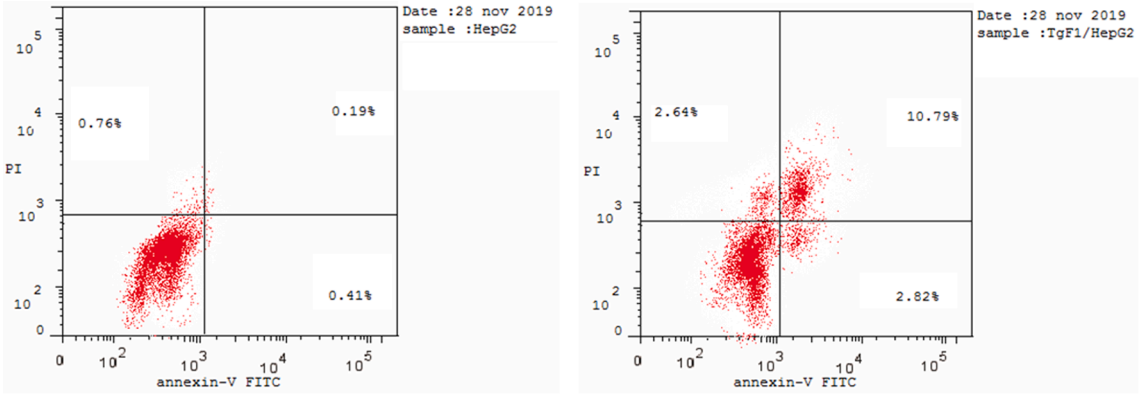

Fig. 10. Flow cytometry analysis of HepG2 cell line treated with DMSO (left) and compound **27f** at 1 μg/mL concentration (right) for 48 h.

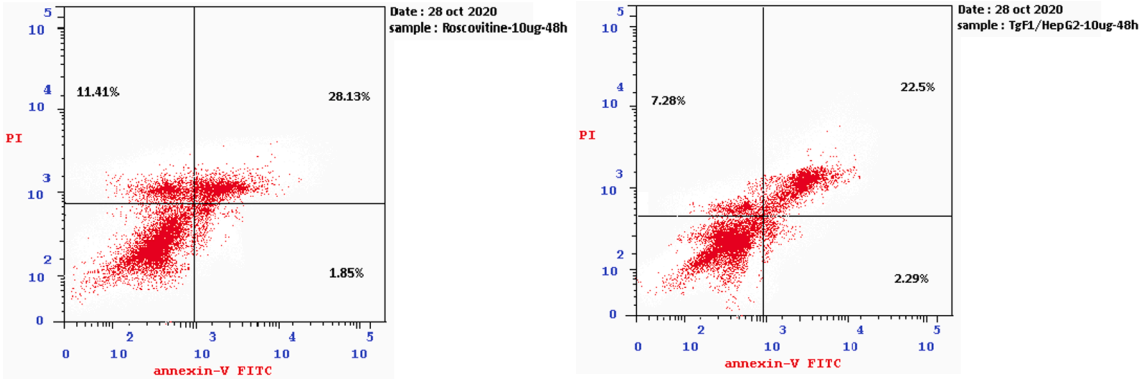

Fig. 11. Flow cytometry analysis of HepG2 cell line treated with Roscovitine at 10 μg/mL concentration (left) and compound **27f** at 10 μg/mL concentration (right) for 48 h.

Table 4
The docking binding free energies of the synthesized compounds against CDK2.

Compound	Binding free energy (kcal/mol)	Compound	Binding free energy (kcal/mol)
25a	−15.63	**27j**	−21.41
27a	−24.22	**27k**	−21.21
27b	−18.65	**27l**	−19.81
27c	−18.27	**27m**	−24.94
27d	−20.68	**27n**	−22.06
27e	−22.67	**27o**	−20.29
27f	−18.63	**27p**	−25.15
27g	−17.88	**27q**	−24.51
27h	−25.03	**27r**	−23.49
27i	−21.69	**Roscovitine**	−17.03

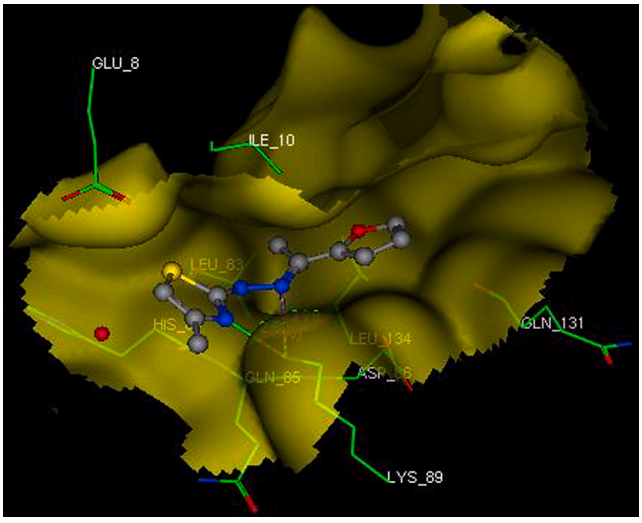

Fig. 12. Calculated binding mode of compound **27f** (grey sticks) within the binding pocket of CDK2 receptor. The active pocket has been represented as yellow surface. Important binding sites residues have been depicted as green sticks. (For interpretation of the references to colour in this figure legend, the reader is referred to the web version of this article.)

5. Experimental

5.1. Chemistry

5.1.1. General

All melting points were determined on a Griffin and Geory melting-point apparatus and were uncorrected. IR spectra were recorded on Pye Unicam SP1200 spectrophotometer using the KBr wafer technique (λ_{max} in cm^{-1}). ^1H NMR spectra were obtained with a Varian Gemini 400 MHz on Bruker Avance III, while ^{13}C NMR spectra were run at 400 MHz. Acquired FIDs were analyzed using ACD/labs software. Tetramethylsilane (TMS) was used as an internal standard in deuterated dimethylsulphoxide (DMSO-d_6). Chemical shifts (δ) are reported in ppm downfield from TMS and coupling constant (*J*) values were reported in Hertz (Hz). Signal multiplicities were represented by s (singlet), d (doublet), t (triplet), q (quadruplet), and m (multiplet). Mass spectra were recorded on a Shimadzu GC–MS-QP 1000X spectrometer operating at 70 e.V. Elemental analyses were carried out at the Microanalytical Unit, Faculty of Science, Ain Shams University, using a PerkinElmer 2400 CHN elemental analyzer, and satisfactory analytical data (±0.4%) were obtained for all compounds. Reactions progression was monitored

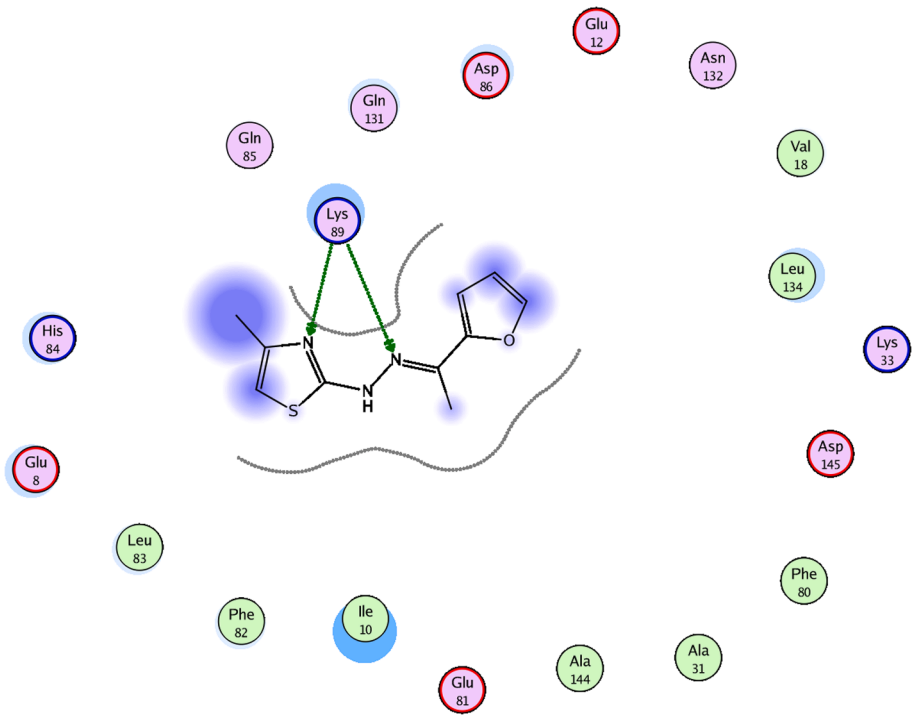

Fig. 13. 2D interaction of compound **27f** with the active site of CDK2.

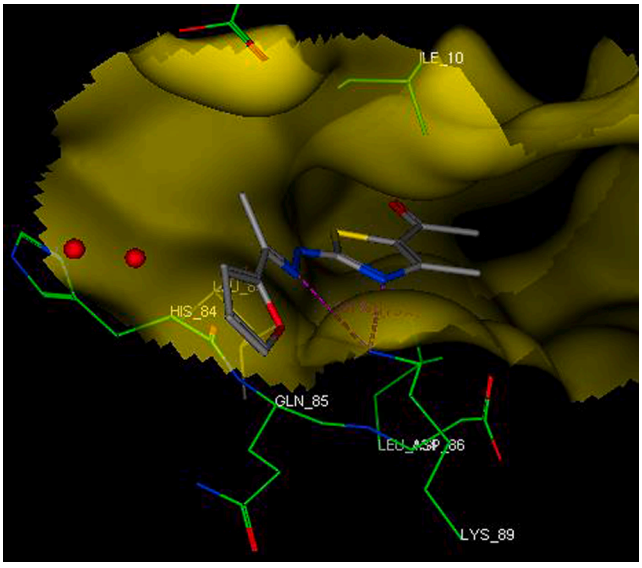

Fig. 14. Calculated binding mode of compound **27g** (grey sticks) within the binding pocket of CDK2 receptor. The active pocket has been represented as yellow surface. Important binding sites residues have been depicted as green sticks. (For interpretation of the references to colour in this figure legend, the reader is referred to the web version of this article.)

by thin layer chromatography (TLC) using aluminum sheet silica gel F254 (Merck). The Microwave reactions were carried out by Microsynth instrument type MA143 (Microwave flux). The ultrasound-assisted reactions were performed in Digital Ultrasonic Cleaner CD-4830 (35 KHz, 310 W).

*5.1.2. General procedure for preparation of arylidene-hydrazinyl-thiazole derivatives **27a-r***

Method A: Under Microwave

A mixture of thiosemicarbazide (**24**, 10 mmol), appropriate aryl ketones (**23a-f**, 10 mmol) namely, 2-acetyl thiophene, 2- acetyl furan, 3,4-dimethoxyacetophenone, 4-methylacetophenone, 4-chloroacetophenone and 2-acetylnaphthalene, respectively, and 2 mL of glacial acetic acid was added to the reaction vessel, placed into the microwave reactor, and allowed to react under microwave irradiation at 200–400 W power and 120° C for 2 min. After the reaction is completed (monitored by TLC). Aliphatic α-halo ketones (**26a-d**, 1.1 mmol) namely, phenacyl bromide, 3- nitro phenacyl bromide, chloroacetone and chloroacetylacetone were dissolved in anhydrous ethanol (10 mL) and added to the reaction vessel. The reaction mixture was then subjected to microwave irradiation at 200–400 W power and 120° C for 2 min. After completion of the reaction and cooling, the product was obtained by filtration and recrystallized from ethanol to give the target compounds (**27a-r**) with an isolated yield of 88–95% which is reported in Table 1.

Method B: Under Sonication

A mixture of thiosemicarbazide (**24**, 10 mmol) and appropriate aryl ketones (**23a-f**, 10 mmol) namely, 2-acetyl thiophene, 2- acetyl furan, 3,4-dimethoxyacetophenone, 4-methylacetophenone, 4-chloroacetophenone and 2-acetylnaphthalene, respectively, in anhydrous ethanol (20 mL) with catalytic amount of acetic acid glacial was placed in Erlenmeyer flask (50 mL) and subjected to ultrasound waves at room temperature for 5 min. Aliphatic α-halo ketones (**26a-d**, 1.1 mmol) namely, phenacyl bromide, 3-nitro phenacyl bromide, chloroacetone and chloroacetylacetone were dissolved in ethanol (10 mL) and added to the reaction vessel. The reaction mixture was then subjected to ultrasound waves at room temperature for 15 min. The precipitated solid was filtered off, dried, and finally recrystallized from ethanol to afford the pure products **(27a-r)** with an isolated yield of 55–79% which is reported in Table 1.

*5.1.2.1. (E)-4-phenyl-2-(2-(1-(thiophen-2-yl)ethylidene)hydrazinyl)thiazole (**27a**).* Yellow crystals; m.p. 258–260 °C; IR (KBr, cm^{-1}): 3219, 3116 (NH), 3030 (CH-aromatic), 2977 (CH aliphatic), 1613 (C═N); ^{1}H NMR (DMSO-d_6) δ ppm: 2.33 (s, 3H, CH_3), 7.05–7.07 (m, 1H, Ar-H $_{of\ thiophene\ ring}$), 7.29 – 7.31 (m, 2H, Ar-H $_{of\ phenyl}$), 7.38–7.40 (m, 3H, Ar-H $_{of\ phenyl}$), 7.52 (s, 1H, Ar-H $_{of\ thiazol\ ring}$), 7.85–7.87 (m, 2H, Ar-H $_{of\ thiophene\ ring}$); Anal. Calcd. for $C_{15}H_{13}N_3S_2$ (299.4): C, 60.17; H, 4.38; N,

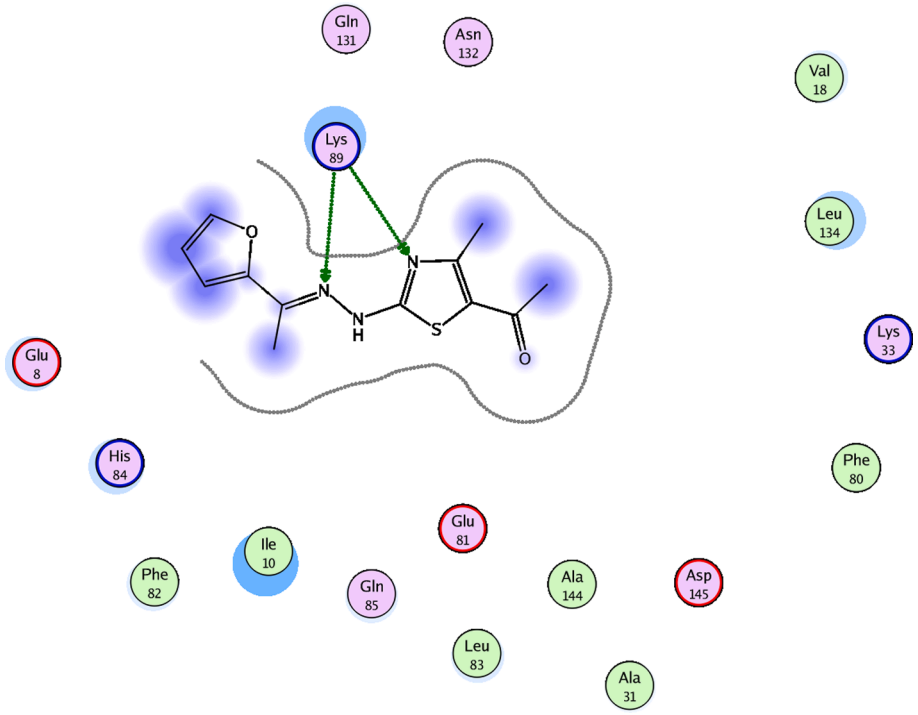

Fig. 15. 2D interaction of compound **27g** with the active site of CDK2.

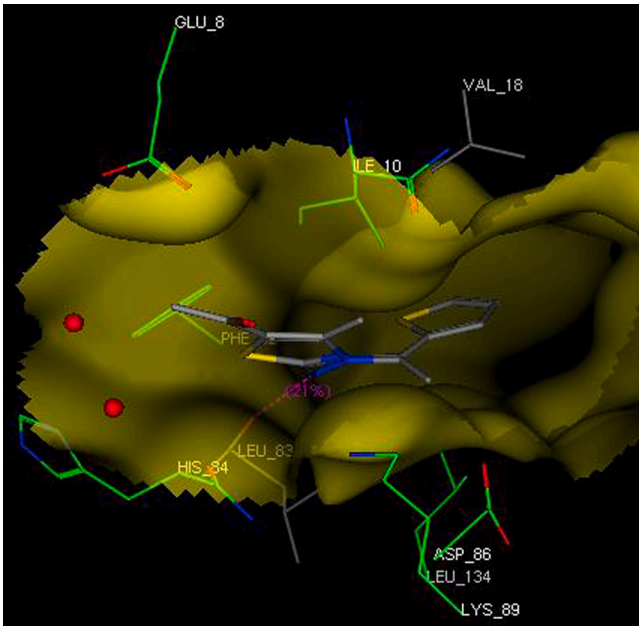

Fig. 16. Calculated binding mode of compound **27c** (grey sticks) within the binding pocket of CDK2 receptor. The active pocket has been represented as yellow surface. Important binding sites residues have been depicted as green sticks. (For interpretation of the references to colour in this figure legend, the reader is referred to the web version of this article.)

14.03; Found: C, 59.88; H, 4.28; N, 13.89.

*5.1.2.2. (E)-4-methyl-2-(2-(1-(thiophen-2-yl)ethylidene)hydrazinyl)thiazole (**27b**).* Yellow crystals; m.p. 200–202 °C; IR (KBr, cm^{-1}): 3387, 3332 (NH), 3064 (CH-aromatic), 2998 (CH aliphatic), 1617 (C═N); ^{1}H NMR (DMSO-d_6) δ ppm: 2.23 (s, 3H, CH_3), 2.43 (s, 3H, CH_3), 6.59 (s, 1H, Ar-H $_{\text{of thiazol ring}}$), 7.10–7.12 (dd, 1H, Ar-H $_{\text{thiophene ring}}$, J = 3.74, 5.05 Hz,), 7.54 (d, 1H, Ar-H $_{\text{thiophene ring}}$, J = 3.08 Hz), 7.63 (dd, 1H, Ar-H $_{\text{thiophene ring}}$, J = 0.88, 5.27 Hz,); MS (*m/z*, %): 238 (M^+ + 1, 21.6), 237 (M^+, 39.6), 232 (25.1), 134.9 (100); Anal. Calcd. for $C_{10}H_{11}N_3S_2$ (237.3): C, 50.61; H, 4.67; N, 17.71; Found: C, 50.43; H, 4.55; N, 17.60.

*5.1.2.3. (E)-1-(4-methyl-2-(2-(1-(thiophen-2-yl)ethylidene)hydrazinyl) thiazol-5-yl)ethan-1-one (**27c**).* Yellow crystals, m.p. 218–220 °C; IR (KBr, cm^{-1}): 3342 (NH), 2919 (CH aliphatic), 1652 (C═O), 1611 (C═N); ^{1}H NMR (DMSO-d_6) δ ppm: 2.33 (s, 3H, CH_3), 2.39 (s, 3H, CH_3), 2.48 (s, 3H, CH_3), 7.06–7.08 (dd, 1H, Ar-H $_{\text{thiophene ring}}$, J = 3.74, 5.05 Hz,), 7.42 (d, 1H, Ar-H $_{\text{thiophene ring}}$, J = 1.10, 3.74 Hz), 7.54–7.55 (dd, 1H, Ar-H $_{\text{thiophene ring}}$, J = 1.10, 5.05 Hz,); Anal. Calcd. for $C_{12}H_{13}N_3OS_2$ (279.4): C, 51.59; H, 4.69; N, 15.04; Found: C, 51.34; H, 4.60; N, 14.89.

*5.1.2.4. (E)-4-(3-nitrophenyl)-2-(2-(1-(thiophen-2-yl)ethylidene)hydrazinyl)thiazole (**27d**).* Yellow crystals; m.p. 246–248 °C; IR (KBr, cm^{-1}): 3215, (NH), 3042, (CH-aromatic), 2924 (CH aliphatic), 1614 (C═N); ^{1}H NMR (DMSO-d_6) δ ppm: 2.28 (s, 3H, CH_3), 7.04 (s, 1H, Ar-H $_{\text{thiazole}}$), 7.32–7.41 (m, 1H, Ar-H $_{\text{nitrophenyl}}$), 7.45–7.52 (m, 1H, Ar-H $_{\text{thiophene ring}}$), 7.62–7.82 (m, 1H, Ar-H $_{\text{nitrophenyl}}$), 7.89 (d, 1H, Ar-H $_{\text{thiophene}}$ J = 3.96 Hz,), 8.15–8.30 (m, 1H, Ar-H $_{\text{nitrophenyl}}$), 8.35 (d, 1H, Ar-H $_{\text{thiophene}}$ J = 7.91 Hz), 8.57–8.78 (m, 1H, Ar-H $_{\text{nitrophenyl}}$); Anal. Calcd. for $C_{15}H_{12}N_4O_2S_2$ (344.4): C, 52.31; H, 3.51; N, 16.27; Found: C, 52.09; H, 3.59; N, 16.16.

*5.1.2.5. (E)-2-(2-(1-(furan-2-yl)ethylidene)hydrazinyl)-4-phenylthiazole (**27e**).* Yellow crystals; m.p. 245–247 °C; IR (KBr, cm^{-1}): 3215, (NH), 3042, (CH-aromatic), 2924 (CH aliphatic), 1614 (C═N); ^{1}H NMR (DMSO-d_6) δ ppm: 2.25 (s, 3H, CH_3), 6.57–6.59 (dd, 1H, Ar-H $_{\text{Furan}}$, J = 1.96, 3.42 Hz), 6.84–6.85 (dd, 1H, Ar-H $_{\text{Furan}}$, J = 0.73, 3.42 Hz), 7.31–7.41 (m, 4H, Ar-H), 7.77 (dd, 1H, Ar-H $_{\text{Furan}}$, J = 0.73, 1.71 Hz), 7.85–7.87 (m, 2H, Ar-H); Anal. Calcd. for $C_{15}H_{13}N_3OS$ (283.3): C, 63.58; H, 4.62; N, 14.83; Found: C, 63.94; H, 4.53; N, 14.72.

*5.1.2.6. (E)-2-(2-(1-(furan-2-yl)ethylidene)hydrazinyl)-4-methylthiazole (**27f**).* Pale yellow crystals; m.p. 238–240 °C; IR (KBr, cm^{-1}): 3221, 3133 (NH), 3096 (CH-aromatic), 2893 (CH aliphatic), 1620 (C═N); ^{1}H

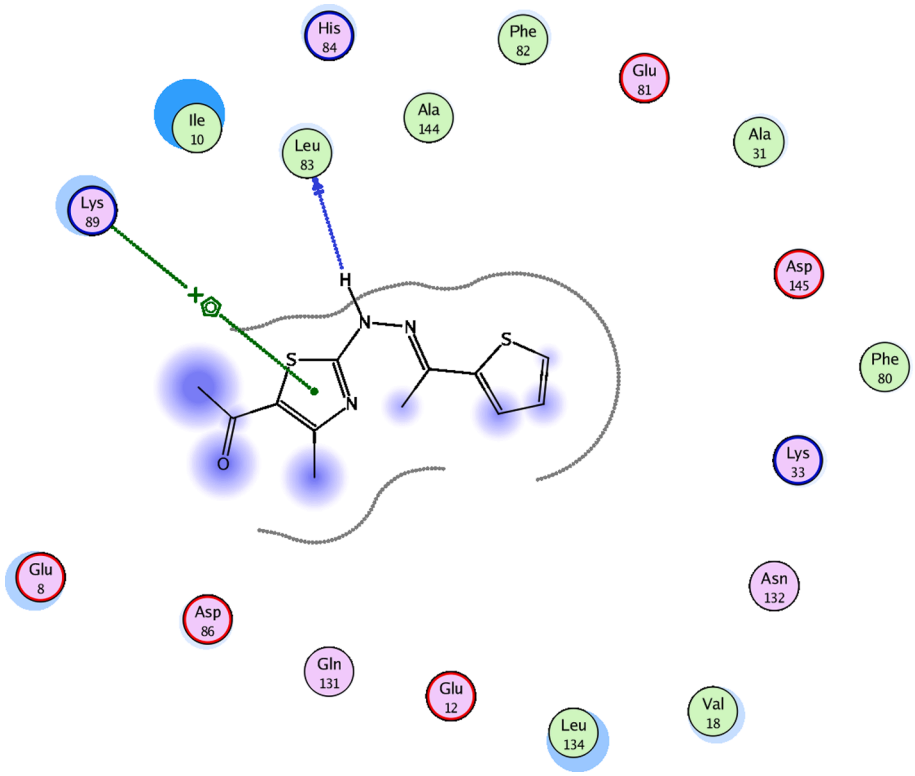

Fig. 17. 2D interaction of compound **27c** with the active site of CDK2.

NMR (DMSO-d_6) δ ppm: 2.22 (s, 3H, CH_3), 2.29 (s, 3H, CH_3), 6.55 (s, 1H, Ar-H $_{\text{of thiazol ring}}$), 6.62–6.63 (dd, 1H, Ar-H $_{\text{thiophene ring,}}$ $J = 1.76$, 3.52 Hz,), 7.00 (br. s, 1H), 7.82 (d, 1H, Ar-H $_{\text{thiophene ring,}}$ $J = 1.32$ Hz); Anal. Calcd. for $C_{10}H_{11}N_3OS$ (221.3): C, 54.28; H, 5.01; N, 18.99; Found: C, 54.18; H, 4.90; N, 18.87.

5.1.2.7. (E)-1-(2-(2-(1-(furan-2-yl)ethylidene)hydrazinyl)-4-methylthiazol-5-yl)ethan-1-one ***(27g)***. Pale yellow crystals; m.p. 215–217 °C; IR (KBr, cm^{-1}): 3416 (NH), 3091 (CH-aromatic), 1684 (C═O), 1612 (C═N); ^{1}H NMR (DMSO-d_6) δ ppm: 2.24 (s, 3H, CH_3), 2.39 (s, 3H, CH_3), 2.49 (s, 3H, CH_3), 6.59 (dd, 1H, Ar-H $_{\text{thiophene ring,}}$ $J = 1.76$, 3.52 Hz,), 6.90–6.91 (dd, 1H, Ar-H $_{\text{thiophene ring,}}$ $J = 0.88$, 3.52 Hz), 7.79 (d, 1H, Ar-H $_{\text{thiophene ring,}}$ $J = 1.32$ Hz); ^{13}C NMR (100 MHz, DMSO-d_6) δ ppm: 13.9, 20.3, 29.4, 110.9, 111.9, 112.0, 143.5, 144.4, 144.5, 151.6, 159.8, 188.7; Anal. Calcd. for $C_{12}H_{13}N_3O_2S$ (263.3): C, 54.74; H, 4.98; N, 15.96; Found: C, 54.65; H, 4.83; N, 15.84.

5.1.2.8. (E)-2-(2-(1-(3,4-dimethoxyphenyl)ethylidene)hydrazinyl)-4-phenylthiazole ***(27h)***. Yellow crystals; m.p. 235–237 °C; IR (KBr, cm^{-1}): 3218 (NH), 3054 (CH-aromatic), 2937 (CH aliphatic), 1628 (C═N); ^{1}H NMR (DMSO-d_6) δ ppm: 2.31 (s, 3H, CH_3). 3.79 (s, 3H, OCH_3), 3.82 (s, 3H, OCH_3), 6.98 (d, 1H, Ar-H, $J = 8.35$ Hz), 7.31–7.39 (m, 3H, Ar-H), 7.41–7.45 (m, 3H, Ar-H), 7.86–7.87 (dd, 2H, Ar-H); Anal. Calcd. for $C_{19}H_{19}N_3O_2S$ (353.4): C, 64.57; H, 5.42; N, 11.89; Found: C, 64.43; H, 5.33; N, 11.77.

5.1.2.9. (E)-2-(2-(1-(3,4-dimethoxyphenyl)ethylidene)hydrazinyl)-4-methylthiazole ***(27i)***. Yellow crystals (yield 82%); m.p. 190–192 °C; IR (KBr, cm^{-1}): 3201, 3119 (NH), 3010 (CH-aromatic), 2942 (CH aliphatic), 1613 (C═N); ^{1}H NMR (DMSO-d_6) δ ppm: 2.26 (s, 3H, CH_3), 3.40 (s, 3H, CH_3), 3.80 (s, 3H, OCH_3), 3.82 (s, 3H, OCH_3), 6.66 (s, 1H, Ar-$H_{\text{thiazole ring}}$), 7.01 (d, 1H, Ar-H, $J = 8.79$ Hz), 7.42 (d, 1H, Ar-H, $J = 8.35$ Hz), 7.52 (s, 1H, Ar-H); ^{13}C NMR (100 MHz, DMSO-d_6) δ 150.6, 148.5, 129.9, 129.4, 123.1, 120.2, 111.2, 110.8, 110.2, 103.8, 55.7, 55.6, 26.4, 15.1; MS (*m/z*, %): 292 ($M^+ + 1$, 2.1), 291 (M^+, 10.6), 291 ($M^{+\cdot}$-1, 1.9), 178 (28.6), 79.0 (100); Anal. Calcd. for $C_{14}H_{17}N_3O_2S$ (291.4): C, 57.71; H, 5.88; N, 14.42; Found: C, 57.58; H, 5.80; N, 14.52.

5.1.2.10. (E)-2-(2-(1-(4-chlorophenyl)ethylidene)hydrazinyl)-4-phenylthiazole ***(27j)***. Off white crystals; m.p. 265–267 °C; IR (KBr, cm^{-1}): 3210 (NH), 3033 (CH-aromatic), 2943 (CH aliphatic), 1618 (C═N); ^{1}H NMR (DMSO-d_6) δ ppm: 2.32 (s, 3H, CH_3), 7.30 (s, 1H, NH), 7.33 (s, 1H, Ar-H $_{\text{thiazole ring}}$), 7.39–7.41 (m, 3H, Ar-H $_{\text{phenyl}}$), 7.47–7.49 (d, 2H, $_{\text{phenyl}}$ $J = 8$ Hz), 7.79–7.81 (d, 2H, Ar-$H_{\text{chlorophenyl}}$, $J = 8.31$ Hz), 7.86–7.88 (d, 2H, Ar-$H_{\text{chlorophenyl}}$, $J = 8$ Hz,); Anal. Calcd. for $C_{17}H_{14}ClN_3S$ (327.8): C, 62.28; H, 4.30; N, 12.82; Found: C, 62.06; H, 4.21; N, 12.70.

5.1.2.11. (E)-2-(2-(1-(4-chlorophenyl)ethylidene)hydrazinyl)-4-methylthiazole ***(27k)***. Off white crystals; m.p. Sublimation at 131–133 °C; IR (KBr, cm^{-1}): 3364, 3125 (NH), 3042 (CH-aromatic), 2933 (CH aliphatic), 1612 (C═N); ^{1}H NMR (DMSO-d_6) δ ppm: 2.26 (s, 3H, CH_3), 2.41 (s, 3H, CH_3), 6.66 (s, 1H, Ar-H $_{\text{of thiazol ring}}$), 7.50–7.52 (dd, 2H, Ar-H $_{\text{Chlorophenyl,}}$ $J = 8.4$ Hz,), 7.94 (d, 2H, Ar-H $_{\text{Chlorophenyl,}}$ $J = 8.35$ Hz); ^{13}C NMR (100 MHz, DMSO-d_6) δ 135.8, 134.4, 130.1, 128.7 (2), 128.4 (2), 128.3, 127.6, 104.0, 15.0, 14.6; Anal. Calcd. for $C_{12}H_{12}ClN_3S$ (265.8): C, 54.23; H, 4.55;N, 15.81; Found: C, 54.05; H, 4.42; N, 15.70.

5.1.2.12. (E)-1-(2-(2-(1-(4-chlorophenyl)ethylidene)hydrazinyl)-4-methylthiazol-5-yl)ethan-1-one ***(27l)***. Yellow crystals; m.p. Sublimation 114–116 °C; IR (KBr, cm^{-1}): 3426 (NH), 2923 (CH aromatic), 2854 (CH aliphatic), 1650 (C═O), 1606 (C═N); ^{1}H NMR (DMSO-d_6) δ ppm: 2.32 (s, 3H, CH_3), 2.40 (s, 3H, CH_3), 2.49 (s, 3H, CH_3), 7.48 (d, 2H, Ar-H $_{\text{chlorophenyl}}$ $J = 8.79$ Hz), 7.82 (d, 2H, Ar-H $_{\text{chlorophenyl}}$ $J = 8.79$ Hz); MS (*m/z*, %): 309 ($M^+ + 2$, 75.7), 307 (M^+, 100), 306 (14.6); Anal. Calcd. for $C_{14}H_{14}ClN_3OS$ (307.8): C, 54.63; H, 4.58; N, 13.65; Found: C, 54.45; H, 4.51; N, 13.53.

5.1.2.13. (E)-4-phenyl-2-(2-(1-(p-tolyl)ethylidene)hydrazinyl)thiazole ***(27m)***. Yellow crystals; m.p. 223–225 °C; IR (KBr, cm^{-1}): 3221 (NH), 3028 (CH-aromatic), 2921 (CH aliphatic), 1619 (C═N); ^{1}H NMR

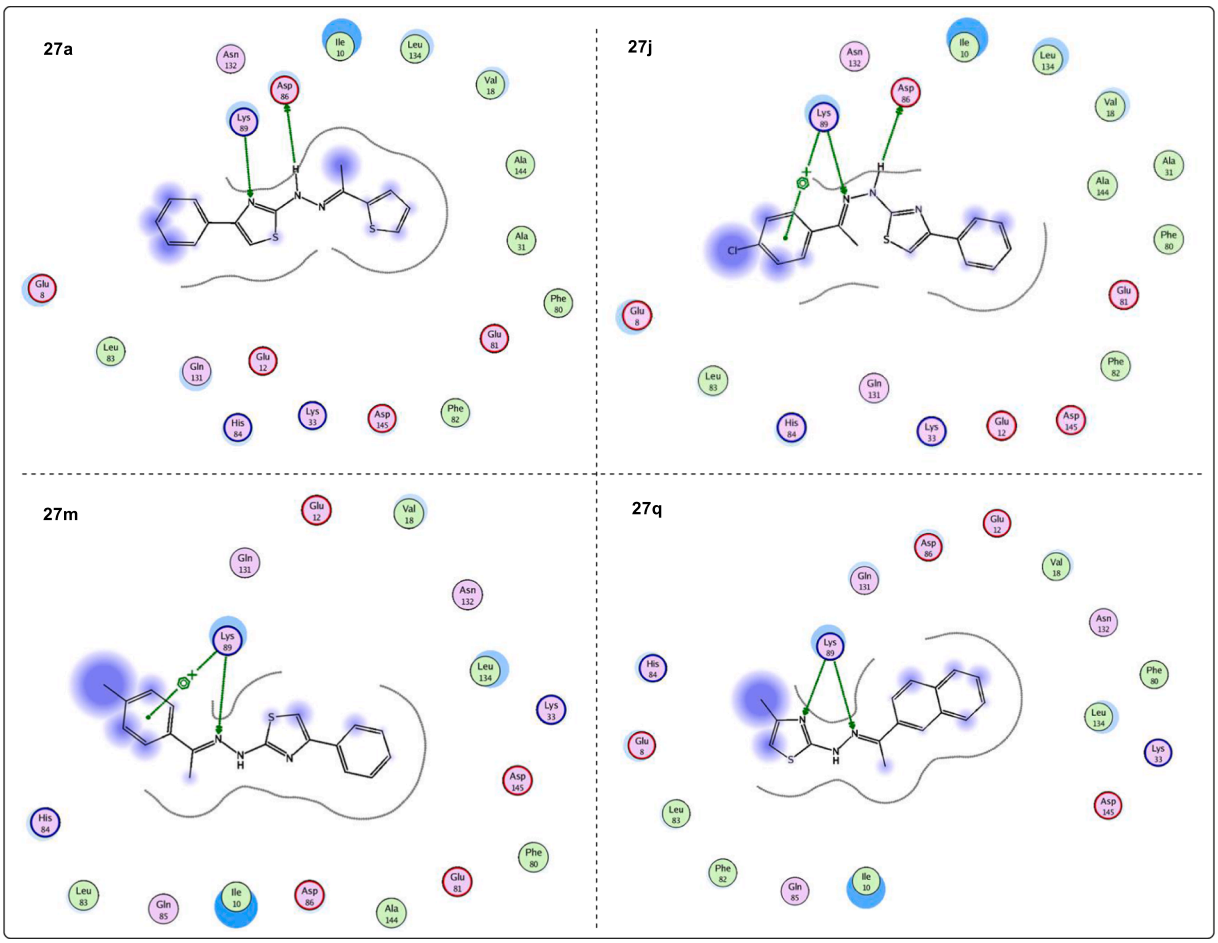

Fig. 18. 2D interaction of compounds **27a, 27j, 27m and 27q** with the active site of CDK2.

(DMSO-d_6) δ ppm: 2.31 (s, 3H, CH_3), 2.33 (s, 3H, CH_3), 7.20–7.24 (m, 2H, Ar-H), 7.30–7.31 (m, 2H, Ar-H), 7.39–7.41 (t, 2H, Ar-H), 7.67–7.69 (m, 2H, Ar-H), *δ* 7.87 (d, 2H, Ar-H, *J* = 7.09 Hz); Anal. Calcd. for $C_{18}H_{17}N_3S$ (307.4):C, 70.33; H, 5.57; N, 13.67; Found: C, 70.09; H, 5.44; N, 13.55.

5.1.2.14. (E)-4-methyl-2-(2-(1-(p-tolyl)ethylidene)hydrazinyl)thiazole ***(27n)***. Yellow crystals; m.p. 148–150 °C; IR (KBr, cm^{-1}): 3387, 3332 (, NH), 3064 (CH-aromatic), 2998 (CH aliphatic), 1613 (C═N); ^{1}H NMR (DMSO-d_6) δ ppm: 2.21 (s, 3H, , CH_3), 2.28 (s, 6H, $2CH_3$), 7.21–7.29 (m, 3H, Ar-H), 7.73 (d, 2H, Ar-H, *J* = 8.35 Hz); MS (*m/z*, %): 245 (M^+, 32.9), 170 (13), 140 (83), 126 (100); Anal. Calcd. for $C_{13}H_{15}N_3S$ (245.3): C, 63.64; H, 6.16; N, 17.13; Found: C, 63.44; H, 6.07; N, 17.05.

5.1.2.15. (E)-1-(4-methyl-2-(2-(1-(p-tolyl)ethylidene)hydrazinyl)thiazol-5-yl)ethan-1-one ***(27o)***. Yellow crystals; m.p.Sublimation 223–225 °C; IR (KBr, cm^{-1}): 3426 (NH), 2919 (CH aliphatic), 1649 (C═O), 1606 (C═N); ^{1}H NMR (DMSO-d_6) δ ppm: 2.30 (s, 3H, CH_3), 2.32 (s, 3H, CH_3), 2.39 (s, 3H, CH_3), 2.50 (s, 3H, CH_3),7.23 (d, 2H, Ar-H, *J* = 8.2 Hz), 7.69 (d, 2H, Ar-H, *J* = 8.2 Hz); Anal. Calcd. for $C_{15}H_{17}N_3OS$ (287.4): C, 62.69; H, 5.96; N, 14.62; Found: C, 62.44; H, 5.84; N, 14.51.

5.1.2.16. (E)-2-(2-(1-(naphthalen-2-yl)ethylidene)hydrazinyl)-4-phenylthiazole ***(27p)***. Off white crystals; m.p. 254–256 °C; IR (KBr, cm^{-1}): 3221 (NH), 3028 (CH-aromatic), 2921 (CH aliphatic), 1619 (C═N); ^{1}H NMR (DMSO-d_6) δ ppm: 2.45 (s, 3H, CH_3), 7.36–7.40 (m, 1H, Ar-H), 7.42 (s, 1H, NH), 7.53–7.55 (m, 4H, Ar-H $_{naphthalene}$), 7.88–7.94 (m, 7H, Ar-H $_{naphthalene}$), 8.21 (s, 1H, Ar-H $_{naphthalene}$); ^{13}C NMR (100 MHz, DMSO-d_6) *δ* 170.2, 135.6, 133.5, 133.3 (2), 129.0, 128.8 (2), 128.7 (2), 128.5, 128.3 (2), 128.2, 127.9, 127.0, 126.9, 125.9, 125.8, 123.5, 14.2; Anal. Calcd. for $C_{21}H_{17}N_3S$ (343.4): C, 73.44; H, 4.99; N, 12.24; Found: C, 73.15; H, 4.89; N, 12.13.

5.1.2.17. (E)-4-methyl-2-(2-(1-(naphthalen-2-yl)ethylidene)hydrazinyl) thiazole ***(27q)***. Yellow crystals; m.p. 179–181 °C; IR (KBr, cm^{-1}): 3379, 3329 (NH), 3051 (CH-aromatic), 2888 (CH aliphatic), 1611 (C═N); ^{1}H NMR (DMSO-d_6) δ ppm: 2.22 (s, 3H, CH_3), 2.45 (s, 3H, CH_3), 7.51–7.53 (m, 2H, Ar-H $_{naphthalene}$ + 1H, s, thiazole), 7.89–7.90 (m, 1H, Ar-H + 1H, s, NH)), 7.97 (d, 2H, Ar-H $_{naphthalene,}$ *J* = 4.83 Hz), 8.18 (d, 1H, Ar-H $_{naphthalene}$), 8.25 (s, 1H, Ar-H $_{naphthalene}$); Anal. Calcd. for $C_{16}H_{15}N_3S$ (281.4): C, 68.30; H, 5.37; N, 14.93; Found: C, 68.09; H, 5.28; N, 14.80.

5.1.2.18. (E)-1-(4-methyl-2-(2-(1-(naphthalen-2-yl)ethylidene)hydrazinyl)thiazol-5-yl)ethan-1-one ***(27r)***. Yellow crystals; m.p. 188–190 °C; IR (KBr, cm^{-1}): 3384, 3221 (NH), 2901 (CH aliphatic), 1649 (C═O), 1610 (C═N); ^{1}H NMR (DMSO-d_6) δ ppm: 2.42 (s, 3H, CH_3), 2.45 (s, 3H, CH_3), 2.52 (s, 3H, CH_3), 7.53–7.55 (dd, 2H, Ar-H, *J* = 6.2, 3.2 Hz, 2H), 7.90–7.94 (dd, 2H, *J* = 9.1, 5.1 Hz), 8.00–8.01 (m, 1H, Ar-H), 8.11 (d, 1H, *J* = 10.5 Hz), 8.24 (d, 1H, *J* = 1.2 Hz); MS (*m/z*, %): (309, 6.2), (127.1, 94.3), 77 (100); Anal. Calcd. for $C_{18}H_{17}N_3OS$ (323.4): C, 66.85; H, 5.30; N, 12.99; Found: C, 66.67; H, 5.22; N, 12.89.

5.2. Biological evaluation

5.2.1. In vitro anti-proliferative activities

The inhibitory effect of the synthesized compounds on cell growth was determined by MTT (3-(4,5-dimethylthiazol-2-yl)-2,5-diphenyltetrazolium bromide) assay. This colorimetric assay is based on the

conversion of the yellow tetrazolium bromide to a purple formazan derivative by mitochondrial succinate dehydrogenase in viable cells. Cell lines were cultured in RPMI-1640 medium supplemented with 10% fetal bovine serum. Antibiotics added were 100 units/ml penicillin and 100 μg/mL streptomycin at 37 °C in a 5% CO_2 incubator. The cell lines were seeded in a 96-well plate at a density of 10^4 cells/well. Cells were allowed to attach and grow for 48 h at 37 °C in a 5% CO_2 humidified atmosphere. After incubation, the cells were treated with different concentration of compounds and incubated for 24 h. After 24 h of drug treatment, 20 μL of MTT solution at 5 mg/mL was added to each well and incubated for 4 h. Dimethyl sulfoxide (DMSO) in volume of 100 μL is added into each well to dissolve the purple formazan formed. The colorimetric assay is measured and recorded at absorbance of 570 nm using a plate reader (EXL 800, USA). The relative cell viability in percentage was calculated as (Absorbance of treated wells/Absorbance of control wells) × 100.

5.2.2. Kinase inhibitory assay

The *in vitro* inhibitory activities of the synthesized compounds against CDK2 were carried out using CDK2/cyclin A kinase assay kit (ADP-Glo™, Promega, USA). ADP-Glo™ Kinase Assay is a luminescent ADP detection assay. The enzyme, substrate, ATP and inhibitors in was diluted in Kinase Buffer (10% v/v). A suitable range of dilutions of the test inhibitor were made from a 10 mM stock (in DMSO), using sterile water with 0.1% DMSO as dilutent. The solutions were made from stock at room temperature and checked for complete solubility of compound (which may precipitate at 4 00. Assays were performed in 1.5 mL Eppendorf tubes. 1 μL of inhibitor or (5% DMSO), followed by 2 μL of enzyme was added to the Eppendorf tube, followed by 2 μL of substrate/ATP mix. After incubation for 10 min at room temperature in a shaking inhibitor, 5 μL of ADP-Glo™ Reagent was added, followed by incubation at room temperature for 40 min. Finally, 10 μL of Kinase Detection Reagent was added, and the mixture was incubated for further 30 min. Then, The IC_{50} values were determined after luminescence record. The CDK1 and EGFR inhibitory assay was conducting using Kinase-Glo MAX (Promega #V6071).

5.2.3. In-vitro DNA-Flow cytometric (cell cycle) analysis

HepG2 cells were plated at 1×10^5 cells in a 10 cm plate and allowed to adhere overnight. Cells were starved for 24 h prior to treatments at 2x the growth inhibition IC_{50} values with **27f**, roscovitine or DMSO and were incubated for 24 and 48 h before cell cycle analyses. 1×810^5 cells were collected and pelleted by centrifugation at 500×g for 5 min at 4 °C. Supernatant was decanted and pellets were resuspended in 1 mL of 70% ethanol and incubated at 4 °C for 1 h. Samples were centrifuged at 500×g for 5 min at 4 °C and ethanol was removed. Pellets were washed 1x with 1 mL of 1xPBS then centrifuged. PBS was removed and samples were resuspended in 200 μL 1X Propidium Iodide + RNase Staining Solution and incubated at 37 °C for 30 min. Cell-cycle distribution was evaluated using a BD FACSCalibur flow cytometer. Data were collected from three individual experiments.

5.2.4. Annexin V-FITC apoptosis assay

Annexin V- FITC apoptosis detection kit (BioVision product, USA) was used to quantify the percentage of cells undergoing apoptosis and to determine the mode of cell death whether by apoptosis or necrosis in the presence or absence of **27f** or roscovitine. The experiment was carried out according to the manufacturer's protocol. Briefly, cells were seeded (1×10^5 –5×10^5) per dish and allowed to adhere overnight in CO_2 incubator. Following 24 h incubation, **27f** was added and plates were incubated for another 24 h in CO_2 atmosphere. Both adherent and nonadherent cells were trypsinized, collected and centrifuged for 5 min at 300g. Cell pellets were washed with 2 mL of cold PBS twice, re-suspended in 500 μL of 1X binding buffer and stained with 5 μL of Annexin V-FITC and 5 μL of PI for 5 min in the dark at room temperature. Following incubation, 1 mL of 1X binding buffer was added and the analysis was done using BD FACSCalibure flow cytometer within an hour.

5.3. Molecular modeling

The crystal structure of human CDK2 was retrieved from the Protein Data Bank (PDB code: 2A4L, resolution 2.4 Å) and considered as target for docking simulation. The docking analysis was performed using MOE software to evaluate the free energies and binding mode of the designed molecules against CDK2. At first, the protein structures were protonated, and the hydrogen atoms were hided. Then, the energy was minimized, and the binding pockets of the protein were defined.

The 2D structures of the synthesized compounds and roscovitine were sketched using ChemBioDraw Ultra 14.0 and saved as MOL format. Then, the saved files were opened using MOE and 3D structures were protonated. Next, energy minimization was applied. Before docking the synthesized compounds, validation of the docking protocol was carried out by running the simulation only using the co-crystallized ligands and low RMSD between docked and crystal conformations. The molecular docking of the synthesized compounds and the co-crystallized ligand was performed using a default protocol; Placement: Triangle Matcher, Rescoring 1: London dG, Refinement: Force field. For each selected compound, thirty independent docking runs were generated using genetic algorithm protocol.

Declaration of Competing Interest

The authors declare that they have no known competing financial interests or personal relationships that could have appeared to influence the work reported in this paper.

Acknowledgement

The authors gratefully acknowledge the environmental development affairs and community service sector of ASU for financial support for this work.

Appendix A. Supplementary data

Spectral data (^1H, ^{13}C NMR, IR, and ESI-MS) are available in a separated file.

Supplementary data to this article can be found online at https://doi.org/10.1016/j.bioorg.2020.104615.

References

[1] World Health Organization: Cancer – Key Facts, 2018. http://www.who.int/news-room/fact-sheets/detail/cancer.
[2] C. Osborne, P. Wilson, D. Tripathy, Oncogenes and tumor suppressor genes in breast cancer: potential diagnostic and therapeutic applications, Oncologist 9 (4) (2004) 361–377.
[3] C.M. Croce, Oncogenes and cancer, New England J. Med. 358 (5) (2008) 502–511.
[4] K.R. Webster, S.D. Kimball, Novel drugs targeting the cell cycle, Emerging Drugs 5 (1) (2000) 45–59.
[5] L. Meijer, Cyclin-dependent kinases inhibitors as potential anticancer, antineurodegenerative, antiviral and antiparasitic agents, Drug Resist. Updates 3 (2) (2000) 83–88.
[6] H. Hochegger, S. Takeda, T. Hunt, Cyclin-dependent kinases and cell-cycle transitions: does one fit all? Nat. Rev. Mol. Cell Biol. 9 (11) (2008) 910–916.
[7] M. Malumbres, Cyclin-dependent kinases, Genome Biol. 15 (6) (2014) 122.
[8] M. Malumbres, M. Barbacid, Mammalian cyclin-dependent kinases, Trends Biochem. Sci. 30 (11) (2005) 630–641.
[9] Y. Gong, S. Deng, M. Zhang, G. Wang, G.Y. Minuk, F. Burczynski, A cyclin-dependent kinase inhibitor (p21WAF1/CIP1) affects thymidine incorporation in human liver cancer cells, Br. J. Cancer 86 (4) (2002) 625–629.
[10] S. Akli, C.S. Van Pelt, T. Bui, L. Meijer, K. Keyomarsi, Cdk2 is required for breast cancer mediated by the low-molecular-weight isoform of cyclin E, Cancer Res. 71 (9) (2011) 3377–3386.
[11] N. Furuno, N. den Elzen, J. Pines, Human cyclin A is required for mitosis until mid prophase, J. Cell Biol. 147 (2) (1999) 295–306.
[12] T.A. Chohan, A. Qayyum, K. Rehman, M. Tariq, M.S.H. Akash, An insight into the emerging role of cyclin-dependent kinase inhibitors as potential therapeutic agents

for the treatment of advanced cancers, Biomed. Pharmacother. 107 (2018) 1326–1341.
[13] S. Lapenna, A. Giordano, Cell cycle kinases as therapeutic targets for cancer, Nat. Rev. Drug Discovery 8 (7) (2009) 547–566.
[14] Y. Li, O. Barbash, J.A. Diehl, 11 - Regulation of the Cell Cycle, in: J. Mendelsohn, J. W. Gray, P.M. Howley, M.A. Israel, C.B. Thompson (Eds.), The Molecular Basis of Cancer (Fourth Edition), W.B. Saunders, Philadelphia, 2015, pp. 165–178.e2.
[15] R.S. Finn, A. Aleshin, D.J. Slamon, Targeting the cyclin-dependent kinases (CDK) 4/6 in estrogen receptor-positive breast cancers, Breast CANCER Res. BCR 18 (1) (2016) 17.
[16] E. Kodym, R. Kodym, A.E. Reis, A.A. Habib, M.D. Story, D. Saha, The small-molecule CDK inhibitor, SNS-032, enhances cellular radiosensitivity in quiescent and hypoxic non-small cell lung cancer cells, Lung Cancer (Amsterdam, Netherlands) 66 (1) (2009) 37–47.
[17] S. Diab, S. Eckhardt, A. Tan, G. Frenette, L. Gore, W. Depinto, J. Grippo, M. DeMario, S. Mikulski, S. Papadimitrakopoulou, A phase I study of R547, a novel, selective inhibitor of cell cycle and transcriptional cyclin dependent kinases (CDKs), J. Clin. Oncol. 25 (18suppl) (2007), 3528–3528.
[18] W. DePinto, X.J. Chu, X. Yin, M. Smith, K. Packman, P. Goelzer, A. Lovey, Y. Chen, H. Qian, R. Hamid, Q. Xiang, C. Tovar, R. Blain, T. Nevins, B. Higgins, L. Luistro, K. Kolinsky, B. Felix, S. Hussain, D. Heimbrook, In vitro and in vivo activity of R547: a potent and selective cyclin-dependent kinase inhibitor currently in phase I clinical trials, Mol. Cancer Ther. 5 (11) (2006) 2644–2658.
[19] M.S. Squires, R.E. Feltell, N.G. Wallis, E.J. Lewis, D.M. Smith, D.M. Cross, J. F. Lyons, N.T. Thompson, Biological characterization of AT7519, a small-molecule inhibitor of cyclin-dependent kinases, in human tumor cell lines, Mol. Cancer Ther. 8 (2) (2009) 324–332.
[20] K.S. Joshi, M.J. Rathos, R.D. Joshi, M. Sivakumar, M. Mascarenhas, S. Kamble, B. Lal, S. Sharma, In vitro antitumor properties of a novel cyclin-dependent kinase inhibitor, P276–00, Mol. Cancer Ther. 6 (3) (2007) 918–925.
[21] K.S. Joshi, M.J. Rathos, P. Mahajan, V. Wagh, S. Shenoy, D. Bhatia, S. Chile, M. Sivakumar, A. Maier, H.H. Fiebig, S. Sharma, P276–00, a novel cyclin-dependent inhibitor induces G1–G2 arrest, shows antitumor activity on cisplatin-resistant cells and significant in vivo efficacy in tumor models, Mol. Cancer Ther. 6 (3) (2007) 926–934.
[22] G. Siemeister, U. Luecking, C. Wagner, K. Detjen, C. Mc Coy, K. Bosslet, Molecular and pharmacodynamic characteristics of the novel multi-target tumor growth inhibitor ZK 304709, Biomed. Pharmacother. 60 (6) (2006) 269–272.
[23] A. Scholz, K. Wagner, M. Welzel, F. Remlinger, B. Wiedenmann, G. Siemeister, S. Rosewicz, K.M. Detjen, The oral multitarget tumour growth inhibitor, ZK 304709, inhibits growth of pancreatic neuroendocrine tumours in an orthotopic mouse model, Gut 58 (2) (2009) 261–270.
[24] S. Emanuel, C.A. Rugg, R.H. Gruninger, R. Lin, A. Fuentes-Pesquera, P.J. Connolly, S.K. Wetter, B. Hollister, W.W. Kruger, C. Napier, L. Jolliffe, S.A. Middleton, The in vitro and in vivo effects of JNJ-7706621: a dual inhibitor of cyclin-dependent kinases and aurora kinases, Cancer Res. 65 (19) (2005) 9038–9046.
[25] T.A. Chohan, H. Qian, Y. Pan, J.Z. Chen, Cyclin-dependent kinase-2 as a target for cancer therapy: progress in the development of CDK2 inhibitors as anti-cancer agents, Curr. Med. Chem. 22 (2) (2015) 237–263.
[26] Y. Hayashi, Pot economy and one-pot synthesis, Chem. Sci. 7 (2) (2016) 866–880.
[27] O.S. Magne, One-pot reactions: a step towards greener chemistry, Curr. Green Chem. 1 (3) (2014) 216–226.
[28] B. Carbain, D.J. Paterson, E. Anscombe, A.J. Campbell, C. Cano, A. Echalier, J. A. Endicott, B.T. Golding, K. Haggerty, I.R. Hardcastle, P.J. Jewsbury, D.R. Newell, M.E. Noble, C. Roche, L.Z. Wang, R.J. Griffin, 8-Substituted O(6)-cyclohexylmethylguanine CDK2 inhibitors: using structure-based inhibitor design to optimize an alternative binding mode, J. Med. Chem. 57 (1) (2014) 56–70.
[29] C.E. Arris, F.T. Boyle, A.H. Calvert, N.J. Curtin, J.A. Endicott, E.F. Garman, A. E. Gibson, B.T. Golding, S. Grant, R.J. Griffin, P. Jewsbury, L.N. Johnson, A. M. Lawrie, D.R. Newell, M.E. Noble, E.A. Sausville, R. Schultz, W. Yu, Identification of novel purine and pyrimidine cyclin-dependent kinase inhibitors with distinct molecular interactions and tumor cell growth inhibition profiles, J. Med. Chem. 43 (15) (2000) 2797–2804.
[30] J. Cicenas, K. Kalyan, A. Sorokinas, E. Stankunas, J. Levy, I. Meskinyte, V. Stankevicius, A. Kaupinis, M. Valius, Roscovitine in cancer and other diseases, Ann. Transl. Med. 3 (10) (2015), 135–135.
[31] M.A. Dickson, G.K. Schwartz, Development of cell-cycle inhibitors for cancer therapy, Curr. Oncol. (Toronto Ont.) 16 (2) (2009) 36–43.
[32] A.C. Rigas, C.N. Robson, N.J. Curtin, Therapeutic potential of CDK inhibitor NU2058 in androgen-independent prostate cancer, Oncogene 26 (55) (2007) 7611–7619.
[33] K. Vermeulen, M. Strnad, V. Krystof, L. Havlicek, A. Van der Aa, M. Lenjou, G. Nijs, I. Rodrigus, B. Stockman, H. van Onckelen, D.R. Van Bockstaele, Z.N. Berneman, Antiproliferative effect of plant cytokinin analogues with an inhibitory activity on cyclin-dependent kinases, Leukemia 16 (3) (2002) 299–305.
[34] K. Johnson, L. Liu, N. Majdzadeh, C. Chavez, P.C. Chin, B. Morrison, L. Wang, J. Park, P. Chugh, H.M. Chen, S.R. D'Mello, Inhibition of neuronal apoptosis by the cyclin-dependent kinase inhibitor GW8510: identification of 3' substituted indolones as a scaffold for the development of neuroprotective drugs, J. Neurochem. 93 (3) (2005) 538–548.
[35] G. Kontopidis, C. McInnes, S.R. Pandalaneni, I. McNae, D. Gibson, M. Mezna, M. Thomas, G. Wood, S. Wang, M.D. Walkinshaw, P.M. Fischer, Differential binding of inhibitors to active and inactive CDK2 provides insights for drug design, Chem. Biol. 13 (2) (2006) 201–211.
[36] S.T. Davis, B.G. Benson, H.N. Bramson, D.E. Chapman, S.H. Dickerson, K.M. Dold, D.J. Eberwein, M. Edelstein, S.V. Frye, R.T. Gampe Jr., R.J. Griffin, P.A. Harris, A. M. Hassell, W.D. Holmes, R.N. Hunter, V.B. Knick, K. Lackey, B. Lovejoy, M. J. Luzzio, D. Murray, P. Parker, W.J. Rocque, L. Shewchuk, J.M. Veal, D.H. Walker, L.F. Kuyper, Prevention of chemotherapy-induced alopecia in rats by CDK inhibitors, Science 291 (5501) (2001) 134–137.
[37] S.K. Kumar, B. LaPlant, W.J. Chng, J. Zonder, N. Callander, R. Fonseca, B. Fruth, V. Roy, C. Erlichman, A.K. Stewart, C. Mayo Phase, Dinaciclib, a novel CDK inhibitor, demonstrates encouraging single-agent activity in patients with relapsed multiple myeloma, Blood 125 (3) (2015) 443–448.
[38] S.R. Whittaker, A. Mallinger, P. Workman, P.A. Clarke, Inhibitors of cyclin-dependent kinases as cancer therapeutics, Pharmacol. Ther. 173 (2017) 83–105.
[39] J. Radek, P. Kamil, K. Vladimir, Cyclin-dependent kinase Inhibitors Inspired by Roscovitine: Purine Bioisosteres, Curr. Pharm. Des. 18 (20) (2012) 2974–2980.
[40] J. Flynn, J. Jones, A.J. Johnson, L. Andritsos, K. Maddocks, S. Jaglowski, J. Hessler, M.R. Grever, E. Im, H. Zhou, Y. Zhu, D. Zhang, K. Small, R. Bannerji, J.C. Byrd, Dinaciclib is a novel cyclin-dependent kinase inhibitor with significant clinical activity in relapsed and refractory chronic lymphocytic leukemia, Leukemia 29 (7) (2015) 1524–1529.
[41] U. Asghar, A.K. Witkiewicz, N.C. Turner, E.S. Knudsen, The history and future of targeting cyclin-dependent kinases in cancer therapy, Nat. Rev. Drug Discovery 14 (2) (2015) 130–146.
[42] S.A. Elmetwally, K.F. Saied, I.H. Eissa, E.B. Elkaeed, Design, synthesis and anticancer evaluation of thieno[2,3-d]pyrimidine derivatives as dual EGFR/HER2 inhibitors and apoptosis inducers, Bioorg. Chem. 88 (2019), 102944.
[43] K.A.M. Abouzid, G.H. Al-Ansary, A.M. El-Naggar, Eco-friendly synthesis of novel cyanopyridine derivatives and their anticancer and PIM-1 kinase inhibitory activities, Eur. J. Med. Chem. 134 (2017) 357–365.
[44] A.M. El-Naggar, M.M. Hemdan, S.R. Atta-Allah, An efficient one-pot synthesis of new coumarin derivatives as potent anticancer agents under microwave irradiation, J. Heterocy. Chem. 54 (6) (2017) 3519–3526.
[45] E.M. Abbass, A.K. Khalil, A.M. El-Naggar, Eco-friendly synthesis of novel pyrimidine derivatives as potential anticancer agents, J. Heterocy. Chem. 57 (3) (2020) 1154–1164.
[46] A.M. El-Naggar, I.H. Eissa, A. Belal, A.A. El-Sayed, Design, eco-friendly synthesis, molecular modeling and anticancer evaluation of thiazol-5(4H)-ones as potential tubulin polymerization inhibitors targeting the colchicine binding site, RSC Adv. 10 (5) (2020) 2791–2811.
[47] M. Ljungman, M.T. Paulsen, The cyclin-dependent kinase inhibitor roscovitine inhibits RNA synthesis and triggers nuclear accumulation of p53 that is unmodified at Ser15 and Lys382, Mol. Pharmacol. 60 (4) (2001) 785–789.
[48] J.H. Chung, F. Bunz, Cdk2 is required for p53-independent G2/M checkpoint control, PLoS Genet. 6 (2) (2010), e1000863.
[49] M. Kolodziej, C. Götz, P.D. Fazio, R. Montalbano, M. Ocker, H.M. Strik, K.J.O. r. Quint, Roscovitine has anti-proliferative and pro-apoptotic effects on glioblastoma cell lines: a pilot study, Oncol. Rep. 34 (3) (2015) 1549–1556.
[50] A.R. Leach, B.K. Shoichet, C.E. Peishoff, Prediction of protein-ligand interactions. Docking and scoring: successes and gaps, J. Med. Chem. 49 (20) (2006) 5851–5855.